Light-Emitting Devices Based on Doped Polymer Thin Films

Chung-chih Wu

A DISSERTATION

PRESENTED TO THE FACULTY

OF PRINCETON UNIVERSITY

IN CANDIDACY FOR THE DEGREE

OF DOCTOR OF PHILOSOPHY

RECOMMENDED FOR ACCEPTANCE

BY THE DEPARTMENT OF

ELECTRICAL ENGINEERING

NOVEMBER 1997

Distribution of this thesis was supported by NSF (ECS-9612281) and DARPA (USAF-TPSU-PU-1464-967)

Abstract

Organic light-emitting devices (OLEDs) made of single-layer doped polymer thin films have been fabricated and studied. In the hole-transport and matrix polymer poly(N-vinylcarbazole) (PVK), different electron-transport and emissive agents are dispersed or blended to make polymer-based thin films capable of bipolar transport and light emission of various colors. Both the photoluminescence and electroluminescence properties are extensively studied. In photoluminescence, efficient transfer of energy can occur from the host to very dilute (~1 wt.%) amounts of emitting materials. Device characteristics are correlated with material properties to understand the operating mechanisms and to optimize the devices. In electroluminescence, excitons appear to be formed at doped emitting centers, rather than in the transport materials. The device performance is found to be a strong function of the composition of the blend thin films, depending on the luminescence efficiency of emitting centers in the host polymer and the relative hole and electron injection/transport abilities.

Various materials have been used as the anode or cathode contacts to the single-layer doped polymer devices. The device characteristics are very sensitive to the surface properties of the indium tin oxide (ITO) anode contact. OLEDs built on the cleaned as-grown ITO contacts are hole-limited because the ITO is less efficient for hole injection than low-work-function metal cathodes for electron injection. We have demonstrated that without degrading the bulk properties of the ITO, the chemical composition of ITO surface layers could be substantially modified by treatment in plasmas of different gases. With an oxygen plasma treatment, the device performance is greatly improved due to enhanced hole injection, while a hydrogen plasma treatment degrades devices. Ultra-violet photoemission spectroscopy (UPS) measurements indicate that oxygen plasma treatment increases the work function while hydrogen plasma treatment reduces the work function of the ITO surface.

Direct integration of OLEDs of different colors has proven difficult because of the weak resistance of organic materials to chemicals used (solvents, acid and water etc.) for patterning and processing the structures and materials. By sealing the organics from the harmful chemicals with carefully designed device structures and by using dry-etching techniques, a method has been developed to sequentially fabricate and therefore integrate devices of different colors onto a single substrate, all with performance similar to discrete OLEDs made on separate substrates. Taking advantage of the thin-film structures and the substrate versatility of both OLEDs and a-Si TFTs, we have also demonstrated the integration of both devices on a rugged, flexible and lightweight steel foil substrate. The TFT in the integration structure successfully provides enough current to drive the OLED.

Acknowledgments

My experience of graduate study at Princeton has been far beyond what I expected. I feel grateful that I have had the opportunity to work with many brilliant and kind people.

I am especially indebted to my research advisor, Prof. James Sturm, for his unconditional support and guidance throughout this work. I am always impressed and inspired by his boundless enthusiasm for research and fearless pursuit of new challenges. This work would not have been possible without technical support from Prof. Richard Register and Prof. Mark Thompson, who were like my co-advisors and were always willing to share their vast knowledge of chemistry and materials. I also wish to express my gratitude to Prof. Sigurd Wagner, Prof. Antoine Kahn and Prof. Stephen Forrest for their invaluable advice and help on research. Prof. Register and Prof. Forrest also served as my thesis readers and provided helpful suggestions for improving the clarity and completeness of this thesis.

Over the past five years, I have had the pleasure to work with Dr. Jonathan Chun, Dr. Jing Tian, Dr. Paul Burrows, Dr. William Chang, Dr. Elena Dana, Dr. Steve Theiss and POEM manager Mike Valenti. They have taught me many useful skills and provided unselfish assistance at various stages of my research.

Many thanks go to former and current members of Prof. Sturm's research group, who have contributed to my research and made our lab a pleasant place to work. Outside of our group, I am indebted to Chen-Jung Chen, Chih-I Wu, Gong Gu and many fellow students in the EMD group for stimulating discussions and assistance.

Finally, and most of all, want to thank my family and my girlfriend, Yaling Lang. Their support and love never let me down and was always there when I needed it most.

Contents

List of Tables

List of Figures

Chapter 1

Introduction

1.1 Overview

The first reports of electroluminescence (EL) in organic semiconductors were by Helfrich and Schneider [1] in 1965 when they applied 100-1000 V to millimeter-sized anthracene crystals and observed luminescence. The high voltage and poor performance of such macroscopic devices limited the practicality and failed to arouse many further studies. Interest in organic EL was revived in 1987 by the work of Tang, VanSlyke, and Chen [2,3] who fabricated their devices with a two-layer single-heterostructure configuration, consisting of thin (~100 nm) evaporated films of electron-transport 8-hydroxyquinoline aluminum (Alq) and hole-transport diamine. Its device structure (Fig. 1.1) consists of organic layers sandwiched between the transparent anode (indium tin oxide, ITO) and the metal cathode. The capability of operating at low voltage (~10V) and high luminance levels made it clear that a manufacturable technology based on organic light emitting devices (OLEDs) could be developed with improved efficiencies and reliability. Further attention was drawn to organic EL in 1990 when similar devices were made by Burroughes et al. [4,5] based on the conjugated polymer poly(*p*-phenylene vinylene) (PPV), thin films of which were formed by spin-coating or other wet-coating techniques. Since there has been increasing interest in polymer-based OLEDs.

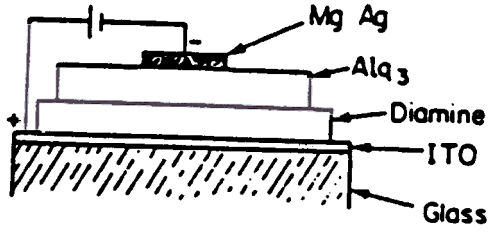

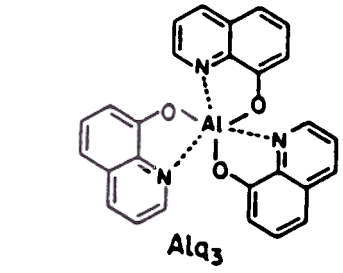

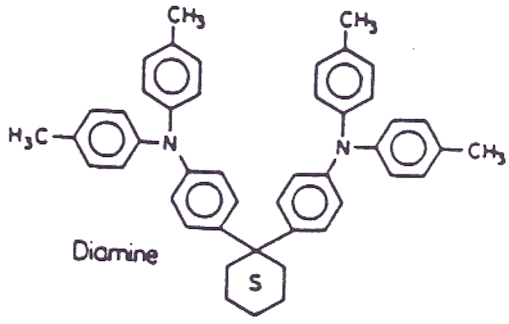

Fig. .1: First practical thin-film organic electroluminescent device, consisting of the Mg:Ag alloy top cathode contact, electron-transport layer (8-hydroxyquinoline aluminum, Alq), hole-transport layer (diamine) and the transparent ITO anode contact. **[2]**

The ability to form thin films of polymers from solutions by convenient wet coating techniques allow them to be deposited on many kinds of substrates, providing opportunities for many novel applications, including displays [6-14].

The inherent thin-film structure of OLEDs make them particularly attractive for flat panel displays (FPD), either as backlighting sources or directly as emitters in emissive displays. Using LEDs to make displays is not new. Alphanumerical displays made of inorganic LEDs have existed for a long time. The requirement of epitaxy of crystalline semiconductors, however, limits the practical growth area. Therefore, large-area LED displays are usually fabricated by expensive and inefficient "pick and place" techniques [13], which also limits the resolution. To allow the fabrication of LED arrays over a large area, there have been efforts to fabricate thin-film LEDs from amorphous inorganic semiconductors, such as a-SiC [15-18]. They have, however, extremely low efficiency and brightness, not nearly enough for practical applications. Therefore, the realization of large-area, high-resolution and cost-effective LED arrays for displays has not been practical until the recent emergence of OLEDs. FPDs made of OLEDs will of course have the inherent advantage of emissive displays, i.e. wide viewing angles, an issue that has long been a weakness of the currently dominant liquid crystal display (LCD) technology. Even compared with other emissive display technologies, OLEDs have many distinctive advantages. One of them is the ease and therefore potentially low cost of fabrication in comparison with inorganic devices. The operating voltages of OLEDs are also apparently much lower than any other emissive display devices. CRTs, thin-film EL [19], plasma displays [20], and field emission displays [21], all require voltages >100V. In addition, the OLED materials provide for mechanical flexibility, which has stimulated the dream of making rollable displays [6, 12-14, 22].

In OLEDs multiple organic materials are usually needed to optimize the functions of electron injection/transport, hole injection/transport, and light emission because luminescent organic materials rarely possess both good hole and electron transport or

injection abilities with available anode and cathode materials. These materials are usually prepared in a layered structure of thin films [23, 24], where each layer performs a different function (Fig. 1.2(a)). With polymers, however, the formation of such multilayer structures is in general more difficult. Extreme care has to be taken with respect to the solvents carrying different layers of materials, so that the solvent carrying a following layer will not dissolve the layers already deposited [25, 26].

Since the polymer thin films are typically coated from solutions, instead of forming multilayers, an alternative method to incorporate the function of different materials into a thin film is to mix all electron-transport, hole transport and emissive materials together in a single solvent and then spin-coat the mixture in a single step, greatly simplifying the fabrication. Such a structure is known as a blend and is illustrated in Fig. 1.2(b). This is a peculiar advantage of polymers, resulting from their solution processibility, and there is no analog of a blend structure for conventional inorganic semiconductors. In a blend, one hopefully preserves the hole transport, electron transport and emissive properties of different materials, despite that they are no longer layered but intimately mixed throughout the film. Devices fabricated in this manner have been demonstrated previously [27-31]. However, in most of these devices, the operating voltage is high, usually up to 30V for light output to be visible. Also, external EL quantum efficiencies are modest, usually on the order of 0.1% (photon/electron). Furthermore, a detailed characterization of this class of devices has not been performed.

This first portion of this thesis is dedicated to the fabrication and understanding of this particular class of devices. The factors that affect device characteristics are investigated to improve device performance. By correlating device characteristics to material properties, we seek to understand the behavior of carriers inside these devices. The second portion addresses some issues in applying these polymer-based devices to display applications, i.e. the integration of OLEDs of different colors in full-color displays and the integration of OLEDs and thin film transistors (TFTs).

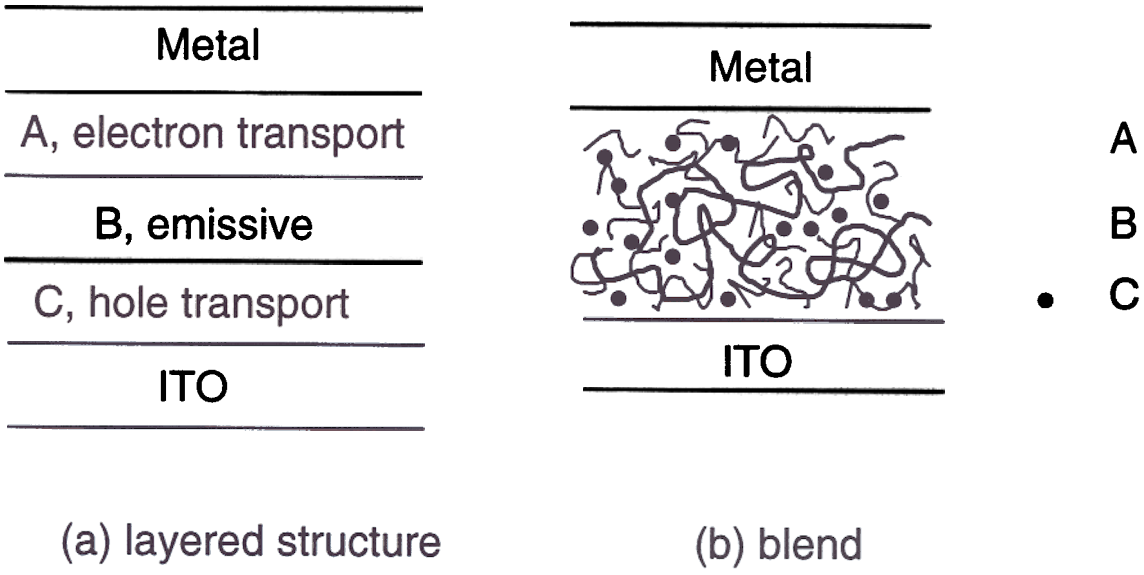

Fig. 1.2: Comparison of (a) an organic EL device with the layered structure and (b) an organic EL device with a single-layer polymer blend thin film.

1.2 Thesis Organization

Chapter 2 serves as an introduction to the physics of organic solids. The electronic structures, optical properties, electrical properties and morphologies of organic molecules and mixed organic solids are visited.

Chapter 3 describes the experimental methods for this thesis work. The preparation and characterization of polymer thin films, the fabrication and characterization of OLED devices, and the photometry usually used in displays or light emitters are discussed.

Chapter 4 examines the properties of single-layer doped polymer thin films and OLEDs made from such materials. Various photophysical phenomena in the thin films are investigated and identified. Electrochemical methods are used to estimate the energy levels (HOMOs and LUMOs) of various materials. The dependence of device performance on the blend composition is systematically studied in a series of devices. By correlating the material properties and device characteristics, the behaviors of charge carriers in devices are studied.

Chapter 5 examines the effect of contacts to devices. First, the effect of plasma treatments on indium tin oxide (ITO) anode contacts are studied. It is found that through an oxygen plasma treatment, the ITO anode contact to doped polymer OLEDs and therefore device performance are substantially improved. To determine the properties of ITO that affect its contact to doped polymers, measurements such as sheet resistance, transmittance, AES, AFM and UPS, have been performed. On the cathode side, the effects of various metal cathodes are studied.

Chapter 6 addresses the integration issues of OLEDs. The first part of this chapter discusses one method to integrate polymer LEDs of three different colors using three organic layers on the same substrate. In the second part of this chapter, the integration of

polymer OLEDs and a-Si TFTs on steel foils is presented, with the top-emitting OLEDs developed for the opaque steel foil substrate.

Chapter 7 summarizes the contributions of this thesis and makes some suggestions for future work.

References

[1] W. Helfrich and W.G. Schneider, Phys. Rev. Lett. **14**, 229 (1965)

[2] C.W. Tang and S.A. VanSlyke, Appl. Phys. Lett. **51**, 913 (1987)

[3] C.W. Tang, S.A. VanSlyke and C.H. Chen, J. Appl. Phys. **65**, 3610 (1989)

[4] J.H. Burroughes, D.D.C. Bradley, A.R. Brown, R.N. Marks, K. MacKay, Friend, P.L. Burn, and A.B. Holmes, Nature **347**, 539 (1990)

[5] D. Braun and A.J. Heeger, Appl. Phys. Lett. **58**, 1982 (1991)

[6] G. Gustafsson, Y. Cao, G.M. Treacy, F. Klavetter, N. Colaneri, and A.J. Heeger, Nature **357**, 477 (1992)

[7] E. Westerweele, P. Smith and A. J. Heeger, Adv. Mater. **7**, 788 (1995)

[8] G. Yu, K. Pakbaz and A.J. Heeger, J. Electron. Materials **23**, 925 (1994)

[9] G. Yu, C. Zhang, and A.J. Heeger, Appl. Phys. Lett. **64**, 1540 (1994)

[10] H.H. Kim, R.G. Swartz, Y. Ota, T.K. Woodward, M.D. Feuer and F. Papadimitrakapolous, Proc. of 1993 IEEE/LEOS Anual Meeting, 202 (1993)

[11] N. Tessler, G.J. Denton and R.H. Friend, Nature **382**, 695 (1996)

[12] P. Yam, Scientific American, 82 (July, 1995)

[13] A.J. Heeger and J. Long Jr., Optics & Photonic News, 23 (Aug., 1996)

[14] P. May, SID Digest of Technical Papers, 192 (May, 1996)

[15] D. Kruangam, T. Endo, M. Deguchi, G.P. Wei, H. Okamoto and Y. Hamakawa, Opto. Devices and Technol. **1**, 67 (1986)

[16] Y. Hamakawa, D. Kruangam, T. Toyama, M. Yoshimi, S. Paasche and H. Okamoto, Opto. Devices and Technol. **4**, 281 (1989)

[17] T.S. Jen, J.Y. Chen, N.F. Shin, J.W. Hong and C.Y. Chang, Electron. Lett. **29**, (1993)

[18] D. Kruangam, Amorphous and Microcrystalline Semiconductor Devices: Optoelectronic Devices (J. Kanicki, Ed.), Artech House, chap. 6 (1991)

[19] C.N. King, J. SID **4**, 1 (1996)

[20] T. Hirose, K. Kariya, M. Wakitani, A. Otsuka and T. Shinoda, SID Digest of Technical Papers, 279 (1996)

[21] F. Courreges, SID Digest of Technical Papers, 45 (1996)

[22] G. Gu, P.E. Burrows, S. Vankatesh and S.R. Forrest, Opt. Lett. **22**, 172, 1997

[23] C.W. Tang, Information Display **12**, 16 (1996)

[24] C. Adachi, S. Tokito, T. Tsutsui and S. Saito, Jap. J. Appl. Phys. **27**, L269 (1988)

[25] I.D. Parker, Q. Pei and M. Marrocco, Appl. Phys. Lett. **65**, 1272 (1994)

[26] J. Pommerehne, H. Vestweber, W. Guss, R.F. Mahrt, H. Bässler, M. Porsch and J. Daub, Adv. Mater. **7**, 551 (1995)

[27] C. Zhang, H. von Seggern, K. Pakbaz, B. Kraabel, H.-W. Schmidt and A.J. Heeger, Synth. Metals **62**, 35 (1994)

[28] C. Zhang, H. von Seggern, B. Kraabel, H.-W. Schmidt, A.J. Heeger, Synth. Metals. **72**, 185 (1995)

[29] G.E. Johnson, K.M. McGrane and M. Stolka, Pure and Appl. Chem.. **67**, 175 (1995)

[30] J. Kido, M. Kohda, K. Okuyama and K. Nagai, Appl. Phys. Lett. **61**, 761 (1992)

[31] J. Kido, H. Shionoya and K. Nagai, Appl. Phys. Lett. **67**, 2281 (1995)

Chapter 2

Physics and Chemistry of Mixed Organic Systems

2.1 Electronic Structures of Molecular Systems

In inorganic semiconductors, the structure is generally characterized by strong covalent or ionic bonding between atoms in the lattice and strong interaction of atomic orbitals in a close-packed structure. In organic solids, the interaction between molecules (or polymer chains in the case of polymers) is comparatively much weaker and the overlap of molecular orbitals is small, so that the molecular energy levels are relatively less disturbed and many features of single molecules are preserved in solids. Most of the electrically or optically active organic compounds contain large conjugated hydrocarbon structures. The term "conjugated" refers to the regular alternation of single and double chemical bonds in the structures. In Fig. 2.1, a few examples are given for small molecules or macromolecules (i.e. polymers) which contain conjugation structures and are frequently used in organic electronics. Pentacene in Fig. 2.1(a) has been used to fabricate p-channel organic thin film transistors with a field effect mobility of >1 $cm^2/V \cdot s$ [1]. The polymer poly(*p*-phenylene vinylene) (PPV) in Fig. 2.1(b) is frequently used in OLEDs [2]. It is conjugated along the polymer chain and belongs to a particular class of polymers called "conjugated polymers". The poly(N-vinyl carbazole) in Fig. 2.1(c) is a hole-transport polymer which has long been used in organic photoconductors

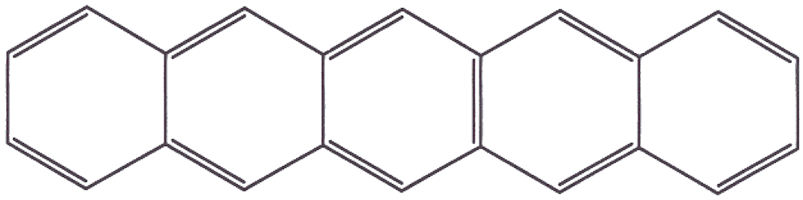

(a) Pentacene

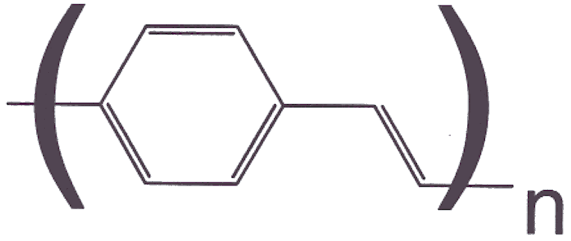

(b) PPV

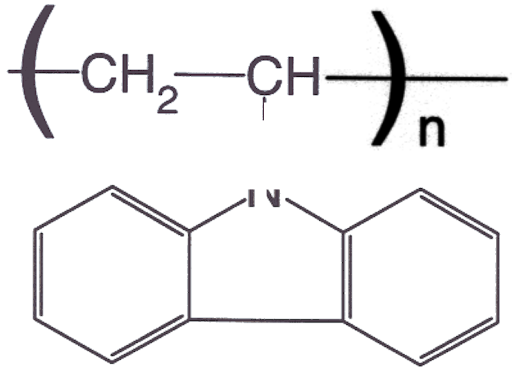

(c) PVK

Fig. 2.1: Chemical structures of (a) pentacene, (b) PPV and (c) PVK.

[3,4] It is not a conjugated polymer, because its polymer backbone is fully "saturated" (i.e. with only single bonds along the main chain) Its optical and electrical activities mainly come from the carbazole groups hanging on the inert polymer backbone. In the carbazole group, again we see the "conjugation" structures.

It is easiest to understand such conjugation structures from a simple example benzene, shown in Fig. 2.2. The "conjugation" of the benzene molecule is manifested in Fig. 2.2(a), where two degenerate representations of benzene are displayed. In Fig. 2.2(b) and Fig. 2.2(c), it is shown that the carbon atom in the benzene molecule has three trigonal sp^2 hybrid orbitals with the interbond angle of 120° on the same molecular plane for σ-bond formation and a lone $2p_z$ orbital with its axis perpendicular to the molecular plane The lone $2p_z$ orbitals overlap to form extended π molecular orbitals (MO) above below the plane. The σ orbitals give localized C-C and C-H bonds The electrons which occupy the σ orbitals are called σ electrons and are strongly localized. The electrons which occupy the π orbitals are called π electrons. π electrons are relatively more loosely bonded and delocalized over the carbon atoms inside the molecule. In a larger conjugated structure, the range of delocalization of π electrons are of course even larger.

The strongly localized σ electrons usually are inert, and many useful optical and electrical properties of such conjugated hydrocarbons are due to the more active π electrons in the π molecular orbitals. Depending on the geometry of the π molecular orbitals, half of them have energy levels lower than the isolated atomic orbital and are occupied [5] These orbitals are called bonding molecular orbitals (i.e. π orbitals). other half have energy levels higher than the isolated atomic orbital and are unoccupied They are called antibonding molecular orbitals (i.e. π* orbitals). Again, the above concepts are illustrated for the benzene in Fig. 2.2(d). Among these MOs, two orbitals are of special significance to the electronic process in conjugated hydrocarbons: the highest occupied molecular orbital (HOMO) because it represents the distribution and

(a)

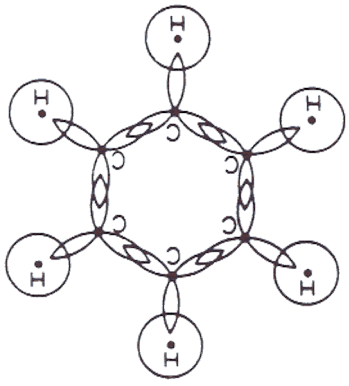

(b)

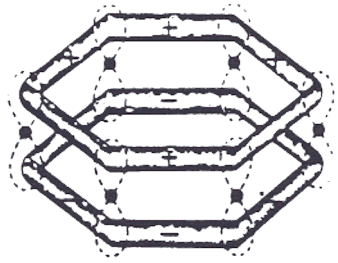

(c)

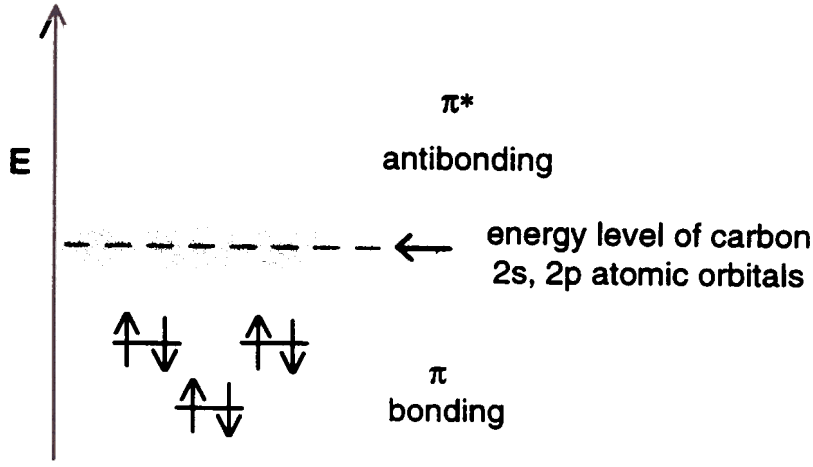

(d)

Fig. 2.2: (a) Two degenerate representations of benzene, (b) The σ hybrids of carbon atoms of benzene, (c) the π-molecular orbitals in benzene, and (d) energy levels of molecular orbitals in benzene [5].

energy of the least tightly held electron in the molecule, and the lowest unoccupied molecular orbital (LUMO) because it describes the easiest route to the excitation of electrons in lower levels or addition of electrons to the system. The energy gap between the LUMO and HOMO of course depends on the size and configuration of the conjugation structure.

2.2 Excited States and Relaxation Processes

In the ground state of a molecule, the electrons fill the HOMO and the LUMO is empty. When the molecule is excited by an external energy source, e.g. light with a sufficient photon energy, an electron in the HOMO can be promoted to the LUMO. Since the occupancy of MOs contributes to the bonding energy, carbon-carbon bond lengths are dependent on the electronic state of the molecule. Therefore, the excitation of a molecule from the ground state to the excited state results in a change in equilibrium geometry of the molecule, and this is observed experimentally through the coupling of electronic and vibrational transitions, as illustrated in Fig. 2.3 [6]. In this figure, the energies of the ground state and excited states are shown as a function of the configuration coordinate of the system, which basically represents the equilibrium positions of the atomic nuclei. In general, the minimum of the excited state potential curve is at a different configuration coordinate to that of the ground state. In each electronic state, there are vibrational sublevels. According to the Born-Oppenheimer approximation, the total wavefunction of a vibrational state can be expressed as the product of the electronic wavefunction and the vibrational wavefunction. Because electronic excitation transitions take place much faster than nuclear motion, there is no change in the nuclear coordinates during an electronic transition. Therefore, electronic transitions are represented by vertical lines in Fig. 2.3 and are known as "vertical" or "Franck-Condon" transitions [6-8]. The probabilities corresponding to the transition to various vibrational excited states in the excited

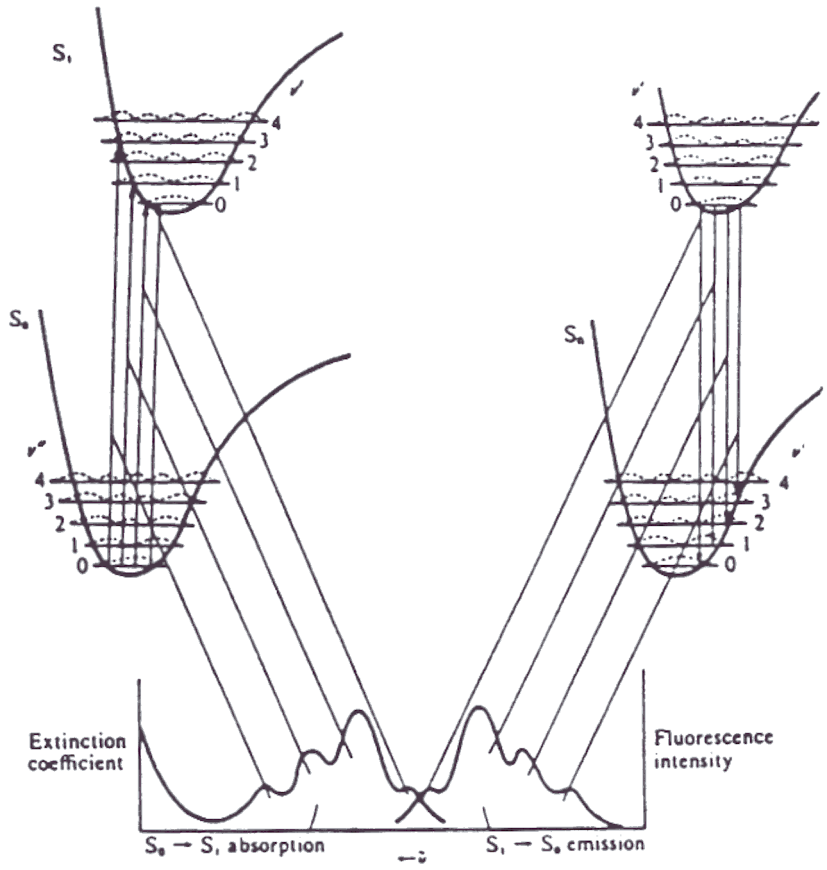

Fig. 2.3: Absorption and emission processes between the ground and excited electronic states of an organic molecule. from Ref.[6])

electronic state are also shown in the same figure. The probability of an electronic transition between two states depends on the overlap between the vibrational wavefunctions of the initial and final states.

A molecule in a vibrationally excited state will undergo radiationless relaxation to the lowest vibrational state. This occurs very quickly compared to the lifetime of the excited electronic state. Therefore radiative decay (i.e. emission) occurs from the lowest vibrational state of the electronic excited state to various vibrational states of the electronic ground state. The emission energy is therefore lower than the absorption energy. The differences between the emission and absorption energies is called the "Franck-Condon shift". In general the reduction of optical energy is called the "Stokes shift" [7]. Thus the Franck-Condon shift is a Stokes shift due to the displacement of the molecule.

In molecular organic solids, the interaction of atoms within a molecule is much stronger than the coupling (van der Waals bonding) between molecules. The electronic excitation of an organic solid is therefore usually similar to that of an isolated molecule. The photoexcitation generates bound electron-hole pairs confined within or near the molecule, i.e. Frenkel excitons, rather than free carriers or Mott-Wannier excitons which could have a large separation between electrons and holes [7]. In the Frenkel model, an excited state of a molecule is basically a state in which an electron has been removed from the filled orbital and occupies a previously empty orbital of higher energy, leaving a hole in the original orbital. When two electrons, one in the ground-state MO and the other in the excited MO, have antiparallel spins, it is in the singlet excited state. When two electrons have parallel spins, it is in the triplet excited state [5]. The corresponding excitons are therefore called singlet or triplet excitons. A schematic energy-configuration diagram for the singlet and triplet excited state is shown in Fig. 2.4, in which the ground singlet state is labeled as S_0, and the nth excited singlet and triplet states are labeled as S_n and T_n. In

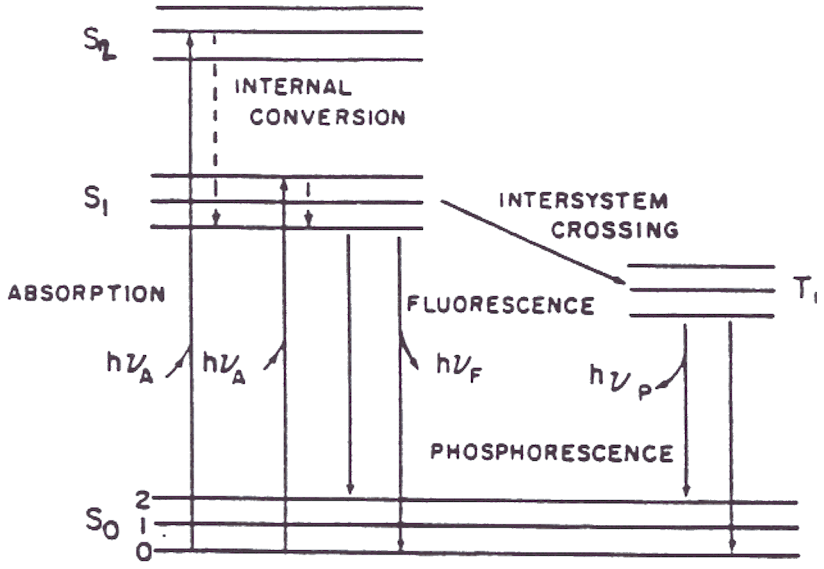

Fig. 2.4: A diagram showing the lowest single and triplet states of a typical molecule and identifying the various transition. (from Ref. [7])

photoexcitation (i.e. absorption), the transition is from the ground singlet state to the excited singlet state.

The radiative transition from S_1 to S_0 (i.e. the lowest radiative decay path of singlet excitons) produces luminescence. However, there are always other transition processes competing with the S_1-S_0 radiative transition. Some important transition processes are listed below [7]:

$S_1 \rightarrow S_0$ + heat	Internal Conversion
$S_1 \rightarrow T_1$ + heat	Intersystem Crossing
$T_1 \rightarrow S_0$ + heat	Intersystem Crossing
$T_1 \rightarrow S_0 + h\nu$	Phosphorescence
$S_1 \rightarrow S_0 + h\nu$	Fluorescence

In general, internal conversion is a non-radiative transition between two states of like spin multiplicity. Intersystem crossing describes the internal conversion (or non-radiative) process involving states of different spin multiplicity. This process occurs between the first excited singlet (S_1) to the first excited triplet (T_1) via a highly vibrating level of T_1 or from T_1 to S_0 via a highly vibrating level of S_0. Of course, after intersystem crossing, phosphorescence may appear due to the T_1 to S_0 radiative transition process, which is a slow process compared to fluorescence because it is a spin-forbidden process. Non-radiative transition processes such as internal conversion, intersystem crossing and impurities-assisted processes reduce the fluorescence (or photoluminescence) yield.

2.3 Morphology of Mixed Systems

The active organic thin films investigated in this thesis are mixed organic thin films prepared by solution casting. In our mixed system, at least one component is a polymer to bind all of the materials together and to allow the preparation of uniform, dense and device-quality thin films from solutions. When only one component is polymer and the

others are small molecules, the molecules are basically dispersed throughout the polymer matrix. When two or more components in the mixture are polymers, the miscibility of polymers becomes an issue. Blends of two or more polymers may be homogeneous or phase separated [9,10]. Whether a particular polymer blend will be homogeneous or phase separated depends on many factors, such as the kinetics of the mixing process, the processing temperatures and the presence of other additives. In general, the primary consideration for determining miscibility of two polymers is a thermodynamic issue that is governed by free-energy considerations.

Blends with separated phases can be organized into a variety of morphologies. For instance, one phase may be dispersed in a matrix of the other or both phases can be continuous. It has been demonstrated that phase-separated polymer blends can be used to produce small light emitting domains in a polymer light emitting diode [11]. The connectivity of phases is also an important morphological feature. If there is interconnection between domains of the same phase, the separated phases form an interpenetrating network of domains, which were found to be beneficial to some types of polymer-based electronic devices. For example, the large interfacial surface area between two interpenetrating charge-transfer polymers has been utilized to facilitate the dissociation of electron-hole pairs generated in photovoltaic cells or photodiodes [12, 13].

2.4 Interaction between Chromophores

On the assumption that the interaction between molecules is weak, the electronic excitation (e.g. absorption) of an organic solid is usually similar to that of an isolated molecule. This situation holds for an organic solid consisting of more than one component if there is no ground-state interaction between different components. The electronic absorption of the mixed system is then the superposition of signals from components. Of course, there are cases in which components in the mixture could interact in the ground

state, for instance the formation of charge-transfer complexes. As a consequence, a change in the electronic absorption is usually detected. In the cases we studied, however, we did not see these phenomena.

The processes considered in the previous section represent only intramolecular transition paths for an excited molecule. In either the single-component or multi-component system, there are, however, other intermolecular interactions which could change the relaxation path of an excited molecule and therefore affect the luminescence [7,14-17]. These are listed as (a)-(d) below:

(a) *Radiative transfer*

This transfer process involves the emission of a photon by the molecule D (donor) and the subsequent reabsorption of this photon by the molecule A (acceptor). The conditions for such an energy transfer process to occur are that the emission spectrum of the molecule D must overlap the absorption spectrum of the molecule A.

(b) *Resonance (Förster) transfer*

The conditions for resonance transfer are the same as those for radiative transfer. But in resonance transfer, no actual emission or absorption of photons takes place. Rather the transition dipole of molecule A produces a field inducing stimulated emission of molecule D. It can be thought of as a process in which molecule A absorbs the photon before molecule D has finished emitting it. This process is also called Förster-type energy transfer.

(c) *Exciton transfer*

Excitons can be thought of as mobile quasi-particles which are neutral in charge. The excitons can therefore move from one molecule to another, to a site in which it either

decays radiatively to produce luminescence or becomes trapped by an impurity molecule with lower energy levels.

(d) *Excimers and exciplexes* [8, 14-17]

An excimer is a dimer or complex formed between an excited chromophore A* and a ground-state chromophore A nearby. Both exciton resonance ($A^*A \leftrightarrow AA^*$) and charge-transfer configurations ($A^+A^- \leftrightarrow A^-A^+$, A^+ and A^- are radical ions of A) contribute to the stabilization of the excimer. Complexes in the excited state are not limited to complexes of identical molecules, that is, excimers; they can also be formed between different molecules through charge transfer between two different chromophores A (acceptor) and D (donors): $A^* + D$ or $A + D^* \rightarrow (A^-D^+)$. Chromophores which tend to form exciplexes usually have relative energy levels as shown in Fig. 2.5. In this figure, it also illustrates schematically the formation of the excited state charge-transfer complexes [18] An excimer or exciplex is best identified by its fluorescence spectrum: a structureless band shifted to longer wavelength from the corresponding monomer emission. This shift is due to stabilization of the complex and to a repulsion energy at the corresponding ground-state configuration, as shown in Fig. 2.6. Fig. 2.6 also shows the configuration relaxation along with the formation of excimers or exciplexes. This dissociated ground state is also responsible for the absence of fine structure in the spectrum. An excimer or exciplex of aromatic molecules usually has a parallel, face-to-face configuration. If the excimers or exciplexes cannot acquire the optimum configuration, then the emission maximum will be shifted to a shorter wavelength than that of a well aligned excimer or exciplex, owing to lower stabilization energy of the complexes

Compared to isolated chromophores, excimers usually have a very low luminescence yield. The formation of excimers strongly depends on the concentration of chromophores in a solvent solution or in a solid solution (i.e. blends). For many organic dyes, pigments or luminescent polymers, the intensity of luminescence falls sharply as the

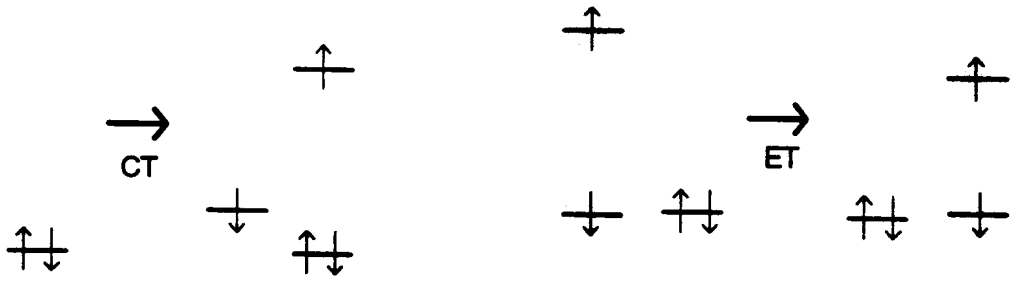

Fig. 2.5: Relative energy levels and schematic illustration for the charge transfer (CT) and energy transfer (ET) mechanism. (from Ref.[18])

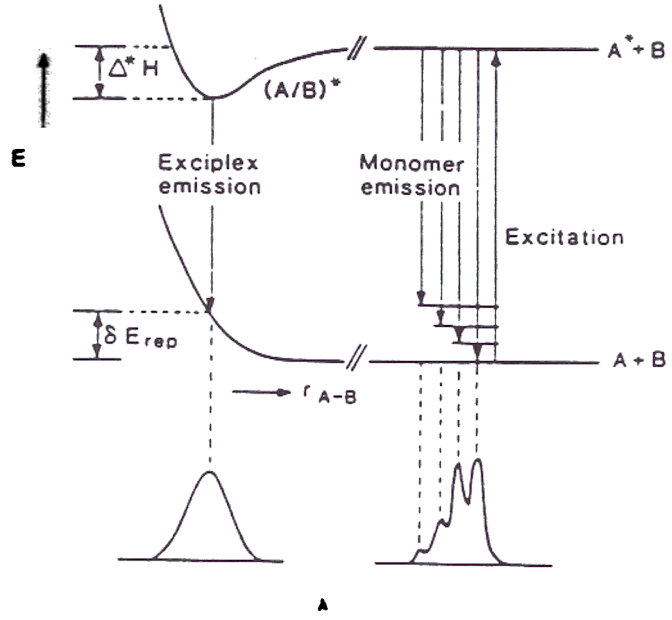

Fig. 2.6: Energy levels of schematic illustration of the formation of excimers and exciplexes and their emission. (from Ref.[14])

chromophore concentration rises [19]. This *concentration quenching* is largely due to the formation of low-quantum-yield excimers.

2.5 Polymeric Systems

The discussion of the electronic structures and the transition processes so far is based on the small molecular weight chromophores. To generalize some of the concepts to polymeric systems requires the understanding of what are the corresponding "chromophores" in the polymeric systems. For polymers with inert backbones and active pendant side groups (e.g. PVK), since each side group can be seen as a "chromophore". the analogy to the small molecule systems is then straightforward. For the conjugated polymers in which the conjugation structure extends over the polymer backbone, the electronic structure is apparently different and one cannot just treat the full polymer chain as a "big chromophore". The physics of conjugated polymers is now reviewed below.

As in the solids of small molecules, the intersite coupling within a polymer chain is much stronger than that between chains, so conjugated polymers are treated as quasi-one dimensional materials [20-24]. Each carbon atom along the length of the conjugated polymer chain contributes one delocalized π electron, and energy bands are formed from the atomic p_z energy levels. Theoretical calculations of the band structures are usually based on the model developed by Su, Schrieffer, and Heeger (SSH model) [20-22].
SSH model considers an isolated infinite polymer chain with cyclic boundary conditions. It involves a tight-binding calculation and the electron-phonon (or electron-lattice) interaction, but neglects the electron-electron interaction (i.e. a one-electron model).
SSH model is therefore a one-dimensional one-electron band model.

Within the description of the SSH model, there is strong coupling between the chain geometry and the occupancy of the π states. As is the case for small conjugated molecules, one can expect a strong coupling between electronic and vibrational

excitations, driven by the different equilibrium geometries in the ground and excited states. The special feature that needs to be considered for the polymers is the length over which these excited states are extended along the chain. The general finding from both theory and experiment is that these states are localized, and the form of this localization depends on the symmetry of the polymer chain [20-23]. Fig. 2.7 illustrates how a conjugated polymer (PPV) chain responds to a charged excitation [23,25,26]. An ideal neutral chain in the ground state would have the intrinsic configuration of Fig. 2.7(a) with a full π (valence) band and an empty π^* (conduction) band. There are no states available in the band gap. Adding one electron onto (Fig. 2.7(b)) or removing one electron from (Fig. 2.7(c)) the chain causes the relaxation (or deformation) of the lattice to an energetically preferable structure. These configurations, consisting of the localized charge accompanied by the local rearrangement of bond alternation, are called polarons. Owing to the localization of this bond rearrangement, the bond alternation "defects" are created in pairs. The interaction between the two confined mid-gap non-bonding p_z levels gives two levels symmetrically displaced about the mid-gap as shown in Fig. 2.7. Therefore, the polarons states are within the energy gap and permit optical transitions at new energies. Spectroscopic methods have been used to demonstrate the existence of these polaron states in a range of polymers [26-29]. Theoretical calculations indicate the extent of the polaron along a polymer chain will be ~10-20 carbon atoms [20,21]. Accommodation of a second charge on one chain through further charging of the "polaron" state gives a doubly charged state, i.e. bipolarons. For the bipolaron, the occupation of the discrete levels within the gap is all empty (charge +2e) or all full (charge -2e), as shown in Fig. 2.8. Also shown in Fig. 2.8 is the neutral excited states formed following photoexcitation or trapping of the electron-hole pairs, which are called polaron-excitons. It has single occupation of each of the two discrete levels in the gap. The transition from the upper to lower level is dipole-allowed in the singlet configuration, while such transition is not allowed in the triplet configuration. The energy levels of the singlet (polaron) excitons are

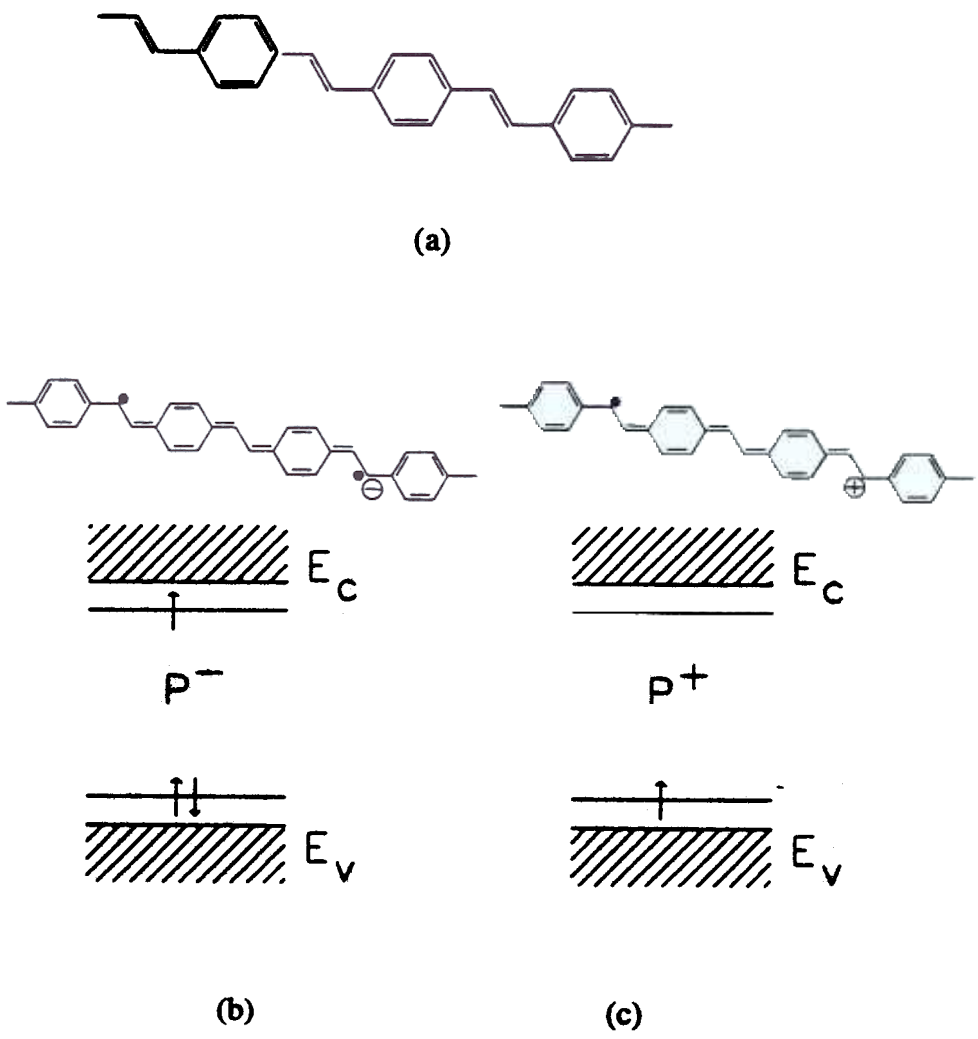

Fig. 2.7: Schematic representation of the formation of polarons on a PPV chain and their energy levels. (a) Intrinsic configuration of a neutral PPV chain in the ground state, (b) a negative polaron P^- and (c) a positive poalron P^+. • represents a non-bonding π electron originally in the chain. $\ominus$ and $\oplus$ represent the added electron and hole. (From Ref. [25])

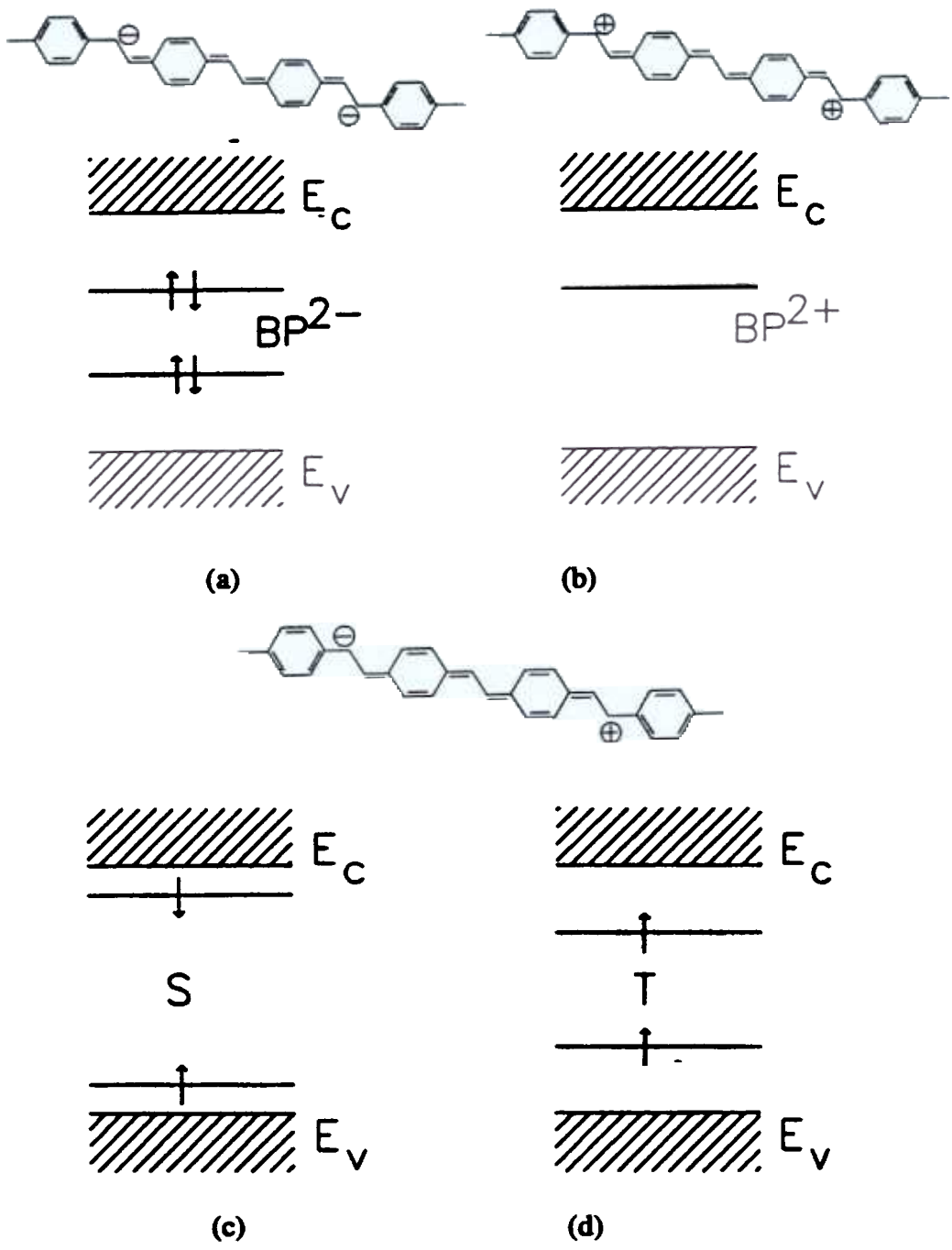

Fig. 2.8: Schematic representation of the formation of bipolarons and polaron-excitons on a PPV chain and their energy levels. (a) a negative bipolaron BP^{2-}, (b) a positive bipoalron BP^{2+}, (c) a singlet polaron-exciton (S) and (d) a triplet polaron-exciton (T). $\ominus$ and $\oplus$ represent the added electron and hole. (From Ref. [25]).

comparable to the polaron levels, but the singlet excitons are usually slightly bound compared two fully separated polarons of opposite signs [30]. In summary, in the luminescent conjugated polymers, the coupling between the π-electron system and the local chain geometry results in a non-linear response to electronic excitation, giving rise to polaron-like self-localized excitations. In all cases, the change in the chain geometry (i.e. bond alternation) has the effect of pulling levels away from the band edges and into the gap.

From the above discussions, the analogy of the photoexcitation and relaxation processes in luminescent conjugated polymers to those in small molecular weight chromophores becomes clear. Through the photoexcitation, localized intrachain (polaron) excitons, analogous to Frenkel excitons in small molecule chromophores, are generated in the conjugated polymers. Because the chain geometries of the ground state and the (polaron) excitons are different, the emission occurs on the low energy side of the absorption. Both absorption and emission spectra show broadening due to vibronic coupling as in the small molecule systems. Although each polymer chain may be hundreds of monomer units long, the polymer chains contain kinks and various defects which interrupt the conjugation sequence. The effective conjugation length in the polymer films is therefore small (on the order of ~10 monomer units) [31-32]. There is also variation in conjugation length among different chain segments. This disorder present in the conjugated polymers results in the inhomogeneous broadening of the absorption spectra. The luminescence spectra are usually comparatively sharper because the excitons can migrate between conjugated segments before recombination [33]. The excitons will move preferentially onto the low-energy segments where they eventually recombine.

The luminescence efficiency of conjugated polymers in the solid state tends to be lower than that measured in dilute solutions, as a result of the exciton migration to quenching sites and also through interchain interactions which produce less radiatively efficient complexes (analogous to excimers or exciplexes discussed earlier) [34,35]. The

sources of quenching sites include the residual impurities from the synthesis routes or chemical defects produced during the processing of a polymer into its final (thin film) form [35]. However, there has been considerable progress made in improving the solid-state luminescence yields in conjugated polymers. The strategies used include: (i) the synthesis of high purity polymers [36], (ii) the use of copolymer structures that incorporate wider energy gap segments to confine excitons and to hinder the migration of excitons to quenching sites [37,38], and (iii) the modification of the polymer structures (e.g. functional side groups) that insure poor packing of the chains to reduce interchain interactions [39]. With these improvements, conjugated polymers with solid-state luminescence yields of 60% to 80% have been reported [36,40,41].

2.6 Charge Transport

The subject of electrical properties of polymer-based materials is extensive. major areas of interest include conjugated polymers, molecularly doped polymers and polymers which have inert polymer chains and electrically active main-chain or side-chain groups [24,42,43]. The electrical properties and the dominant transport mechanisms of these major groups can be very different because of fundamental differences in bonding, morphology or structures. In the conjugated polymers, although the large range of π-electron delocalization may form bands, the charge in a conjugated polymer however exists in polaronic states, which are localized. The transport of polarons may be through "hopping" between sites and render charge transport an activated process [44,45,46]. Such processes are similar to those occurring in the molecularly doped polymers or non-conjugated polymers with pendant active groups. In the following, the discussions will be restricted to molecularly doped polymers and non-conjugated polymers with pendant active groups, the materials on which the major work of this thesis is based. In addition, most available transport data in polymeric systems come from these two systems.

pendant active groups are usually large, planar π-electronic systems. The weak interaction of the π-electronic systems along saturated polymer chains suggests that very little difference should exist in the properties of these polymers and dispersions of analogous molecules in inert polymer matrices. Since these active elements are isolated from one another, classical semiconductor theories of band transport do not apply well. It is now commonly accepted that migration of both electrons and holes involves "hopping", i.e. a sequence of transfers of charges among localized sites [43,47]. These localized sites are associated with individual molecules or functional groups in the polymer chains.

The charge transport properties of these polymers and molecularly doped polymers have been a subject of extensive studies because of their applications as photoconductors for xerography or electrophotography. Since most of these materials absorb only ultra-violet radiation and do not absorb visible light, in most practical organic photoconductors, a layered structure as shown in Fig. 2.9 is usually used [42, 43]. In this structure, visible light penetrates the thick carrier-transport layer and is absorbed in a very thin carrier generation layer. The carrier generation layer usually consists of a highly absorbing layer of a photoconductive material such as amorphous selenium (a-Se), an organic pigment, or

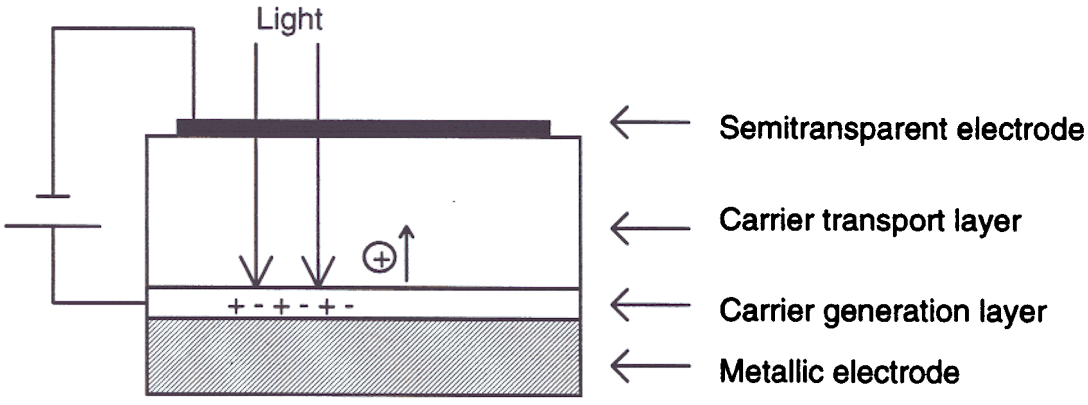

Fig. 2.9: A scheme for a layered photoconductor.

an organic dye. Photogenerated electron-hole pairs are separated by the electric Depending on the polarity of the applied field, one type of carrier is injected into and drifts through the carrier transport layer to the upper electrode, and the other type of carrier leaves the device at the bottom electrode. By choosing the polarity of the applied field, the transport properties of electrons and holes can be studied separately. With such a structure, the transport properties are often studied by the time-of-flight or transit-time technique, in which a thin unipolar carrier sheet is injected at one end of the transport layer after exposure to a short light pulse. The transit time t_T for the sheet of charge to drift across the sample under the influence of a bias field is measured. A drift mobility μ_d is then derived from the transit time t_T, the applied electric field E and the sample thickness L via:

$$\mu_d = L/(t_T \times E)$$

The mobilities measured this way usually show dependence on the electric field, the temperature and the concentration of functional groups or molecules in the film.

In the following, a review of experimental results in the literature for materials relevant to this thesis work is given. The most relevant results are probably those for the hole transport polymer poly(N-vinyl carbazole) (PVK), and for PVK in which the electron transport molecule, 2,4,7-trinitro-9-fluorenone (TNF) is dispersed. Their chemical structures are shown in Fig. 2.10(a). Fig. 2.10(b) and Fig. 2.10(c) show the field dependence of the room-temperature drift mobilities for electrons and holes, respectively for a range of TNF:PVK molar ratios [47] Both hole and electron mobilities increase with the electric field and show an empirical relation of the form:

$$\mu \propto \exp[\gamma E^{1/2}]$$

This empirical dependence has also been observed in a variety of similar systems [48-52] The dependence of μ on $E^{1/2}$ seems consistent with the Poole-Frenkel formalism of field-lowering of hopping barriers [47, 52]. However, there are serious objections to such a model [47]. For instance, the Poole-Frenkel model requires a very high density of charged

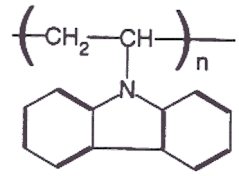

PVK

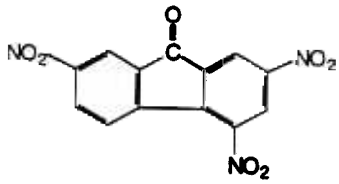

TNF

(a)

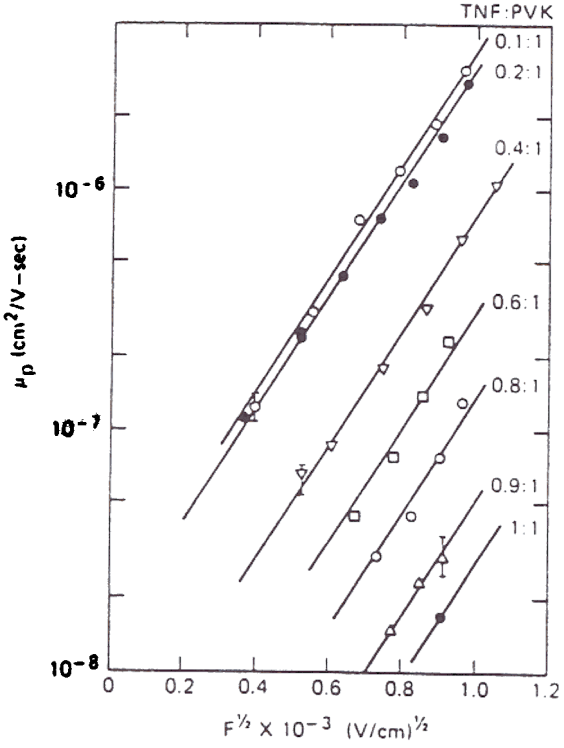

(b)

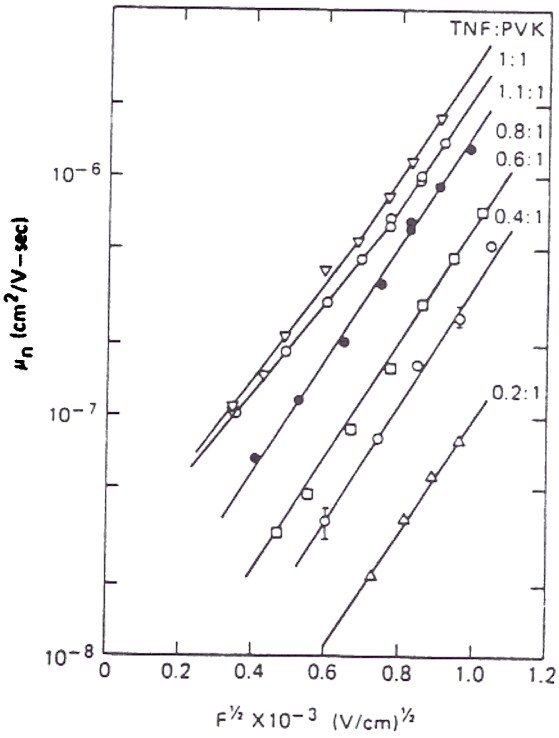

(c)

Fig. 2.10: (a) Chemical structures of PVK and TNF and field dependence of (b) hole drift mobilities and (c) electron drift mobilities for a range of TNF:PVK molar ratios at T = 24 °C. (from Ref.[47])

centers of both polarities, an unrealistic situation in these materials. In general, the relationship between μ and E has not yet been completely elucidated. In Fig. 2.11, the variation of the hole and drift mobility with TNF:PVK compositions is displayed [47]. The electron mobility increases as the TNF concentration increases. It shows that bipolar transport properties can be actually obtained in an organic solid through the blending of two materials which both have only unipolar transport ability. It should be noted that the hole mobility of the matrix polymer PVK is perturbed by the addition of the electron transport agent TNF and decreases as the TNF concentration increases.

Most organic carrier transport materials are hole transport materials. Only a few classes of materials have been found to conduct electrons reasonably well. One important class is oxadiazoles, which have been the major electron transport compounds used in this thesis work. The only available drift mobility data for this class of materials can be found in ref. [53]. Fig. 2.12 shows the chemical structures of different oxadiazole compounds and their mobilities vs. their concentrations in the electrically inert polymer polycarbonate (PC). The strong dependence of the mobilities on the concentration, of course, is expected from the charge hopping nature of molecularly doped polymers.

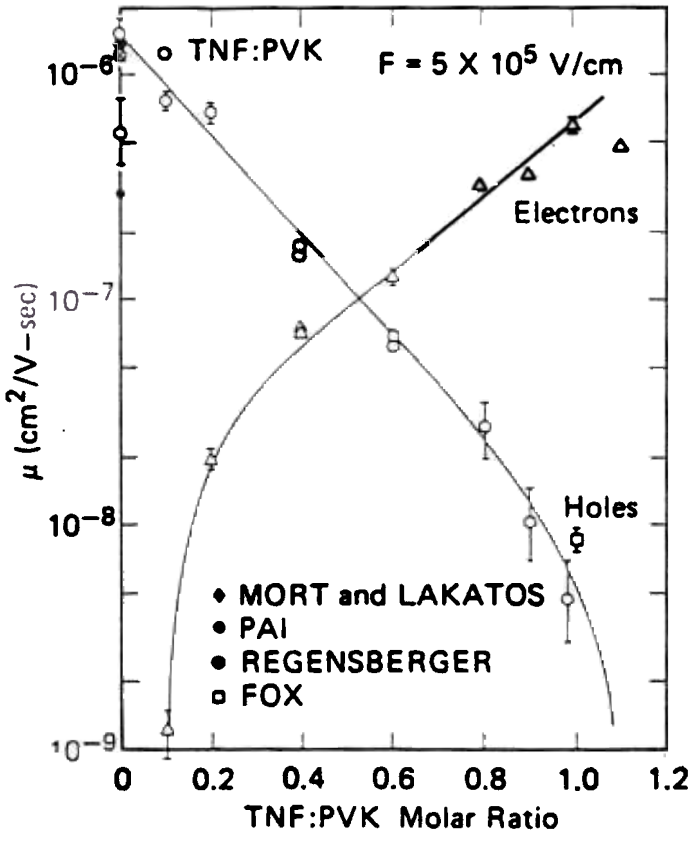

Fig. 2.11: Variation of hole and electron drift mobility with TNF:PVK molar ratio. (from Ref.[47])

(a)

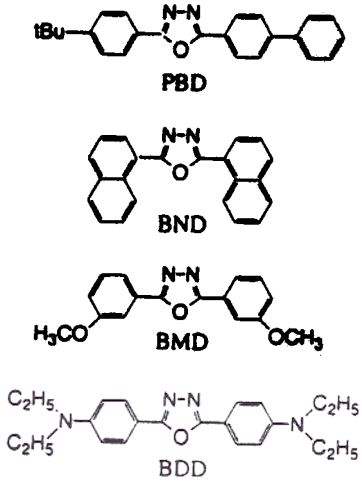

(b)

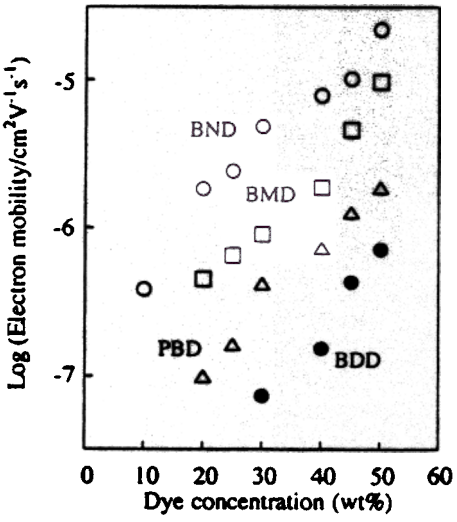

Fig. 2.12: (a) Chemical structures of various oxadiazole compounds, and (b) the concentration dependence of electron drift mobility of oxadiazole compounds dispersed in PC, at an applied field of 7.5×10^5 V/cm at room temperature. (from Ref.[53])

References

[1] Y.Y. Lin, D.J. Gundlach and T.N. Jackson, Tech. Digest of 54th Device Research Conference, Santa Barbara, CA, 80 (1996)

[2] J.H. Burroughes, D.D.C. Bradley, A.R. Brown, R.N. Marks, K. MacKay, R.H. Friend, P.L. Burn and A.B. Holmes, Nature **347**, 539 (1990)

[3] H. Hoegl, J. Phys. Chem. **69**, 755 (1965)

[4] P.J. Regensburger, Photochem. Photobiol. **8**, 429 (1968)

[5] H. Meier, Organic Semiconductors, Verlag Chemie, GmbH, Weinheim (1974)

[6] A. Kearwell and F. Wilkinson, Transfer and Storage of Energies by Molecules, Vol , Wiley, New York (1969)

[7] K.C. Kao and W. Hwang, Electrical Transport in Solids, Pergamon Press Inc. (1981)

[8] N.C. Greenham and R.H. Friend, Semiconductor Device Physics of Conjugated Polymers, Solid State Physics **49**, 1 (1995)

[9] J.R. Fried, Polymer Science and Technology, Prentice-Hall Inc. (1995)

[10] D.R. Paul, S. Newman (ed.), Polymer Blends, Academic Press (1978)

[11] M. Granström and O. Inganäs, Adv. Mater. **7**, 1012 (1995)

[12] S.C. Moratti and A.B. Holmes, Nature **376**, 498 (1995)

[13] G. Yu and A.J. Heeger, J. Appl. Phys. **78**, 4510 (1995)

[14] S.L. Mattes and S. Farid, Science **226**, 917 (1984)

[15] S.A. Jenekhe and J.A. Osaheni, Science **265**, 765 (1994)

[16] J.A. Osaheni and A. Jenekhe, Macromolecules **27**, 739 (1994)

[17] F. Gutmann and L.E. Lyons, Organic Semiconductors, Robert E. Krieger Publishing Company, Malabar, Florida, USA (1983)

[18] F. Papadimitrakopoulos, R.C. Haddon, M. Yan, T.M. Miller, L.J. Rothberg, H.E. Katz and M.E. Galvin, Polymeric Materials Science and Engineering **72**, 455 (1995)

[19] Verlagsgesellschaft mbh, Federal Republic of Germany (1988)

[20] W.P. Su, J.R. Schrieffer and A.J. Heeger, Phys. Rev. Lett. **42**, 1698 (1979)

[21] W.P. Su, J.R. Schrieffer and A.J. Heeger, Phys. Rev. B **22**, 2099 (1980)

[22] A.J. Heeger, S. Kivelson, J.R. Schrieffer and W.P. Su, Rev. Mod. Phys. **60**, 781 (1988)

[23] N. Greenham and R.H. Friend, Semiconductor Device Physics of Conjugated Polymers, Solid State Physics, Vol. **49** (edited by H. Ehrenreich and F. Spaepen), Academic Press (1995)

[24] T.A. Skotheim, Handbook of Conducting Polymers, Marcel Dekker Inc. (1986)

[25] S. Karg, Ph.D. Thesis, University of Bayreuth, 1995

[26] R.H. Friend, D.D.C Bradley and T.D. Townsend, J. Phys. D: Appl. Phys. **20**, 1367 (1987)

[27] J.H. Burroughes, C.A. Jones and R.H. Friend, Nature **347**, 539 (1990)

[28] N.F. Colaneri et al., Phys. Rev. B **42**, 18, 11670 (1990)

[29] K.E. Ziemelis, A.T. Hussain, D.D.C. Bradley, R.H. Friend, J. Rühe and G. Wegner, Phys. Rev. Lett. **66**, 2231 (1991)

[30] J.-L. Brédas, Jérôme Cornil and A.J. Heeger, Adv. Mater. **8**, 447 (1996)

[31] B. Tian, G. Zerbi and K. Müllen, J. Chem Phys. **95**, 3198 (1991)

[32] H.S. Woo, O. Lhost, S.C. Graham, D.D.C. Bradley, R.H. Friend, C. Quattrocchi, J.L. Brédas, R. Schenk and K. Müllen, Synth. Met. **59**, 13 (1993)

[33] M. Gailberger and H. Bässler, Phys. Rev. B **44**, 8643 (1991)

[34] J.W.P. Hsu, M. Yan, T.M. Jedju, L.J. Rothberg and B.R. Hsieh, Phys. Rev. B **49**, 712 (1994)

[35] L.J. Rothberg, M. Yan, F. Papadimitrakopoulos, M.E. Galvin, E.W. Kwock and T.M. Miller, Synth. Met. **80**, 41 (1996)

[36] J.C. Carter, I. Grizzi, S.K. Heeks, D.J. Lacey, S.G. Latham, P.G. May, O. Ruiz de los Paños, K. Pichler, C.R. Towns and H.F. Wittmann, Appl. Phys. Lett. **71**, 34 (1997)

[37] D. Braun, E.G.J. Staring, R.C.J.E. Demandt, G.L.J. Rikken, Y.A.R.R. Kessener and A.H.J. Venhuizen, Synth. Met. **66**, 75 (1994)

[38] P.L. Burn, A.B. Holmes, A. Kraft, D.D.C. Bradley, R.H. Friend and R.W. Gymer, Nature **356**, 47 (1992)

[39] S. Son, A. Dodabalapur, A.J. Lovinger and M.E. Galvin, Science **269**, 376 (1995)

[40] M.A. Díaz-García, F. Hide, B.J. Schwartz, M.D. McGehee, M.R. Andersson and A.J. Heeger, Appl. Phys. Lett. **70**, 3191 (1997)

[41] Q. Pei and Y. Yang, J. Am. Chem. Soc. **118**, 7416 (1996)

[42] J. Mort and D.M. Pai (ed.), Photoconductivity and Related Phenomena, Elsevier Scientific Publishing Company (1976)

[43] J.A. Chilton and M.T. Goosey, Special Polymers for Electronics and Optoelectronics, Chapman & Hall (1995)

[44] L.B. Schein, Phil. Mag. B **65**, 795 (1992)

[45] M. Abkowitz, H. Bässler and M. Stolka, Phil Mag. B **63**, 201 (1991)

[46] G. Paasch, W. Rieβ, S. Karg, M. Meier and M. Schwoerer, Synth. Met. **67**, 177 (1994)

[47] W.D. Gill, J. Appl. Phys. **43**, 5033 (1972)

[48] L.B. Lin, S.A. Jenekhe and P.M. Borsenberger, Appl. Phys. Lett. **69**, 3495 (1995)

[49] P.M. Borsenberger, W.T. Gruenbaum and E.H. Magin, Jpn. J. Appl. Phys. **35**, 2698 (1996)

[50] W.T. Gruenbaum, E.H. Magin and P.M. Borsenberger, Jpn. J. Appl. Phys. **35**, 2704 (1996)

[51] T. Mori, E. Sugimura and T. Mizutani, J. Phys. D: Appl. Phys. **26**, 452 (1993)

[52] L.B. Schein, A. Rosenberg and S.L Rice, J. Appl. Phys. **60**, 4287 (1986)

[53] H. Tokuhisa, M. Era, T. Tsutsui and S. Saito, Appl. Phys. Lett. **66**, 3433 (1995)

Chapter 3

Experimental Methods

3.1 Material Preparation and Characterization

Materials

Fig. 3.1 lists the chemical structures of the organic materials used in this thesis work. The hole-transport polymer PVK, having a high weight-average molecular weight M_W of 1,100,000 g/mole reported by the supplier, was purchased from Aldrich Chemical Inc. and used as received. PVK has a good film-forming property and has been used as the major matrix polymer throughout this thesis work. Electron-transport molecules, 2-(4-biphenyl)-5-(4-tert-butylphenyl)-1,3,4-oxadiazole (PBD), 2,5-bis(4-naphthyl)-1,3,4-oxadiazole (BND) and tris(8-hydroxyquinoline)aluminum (Alq) were purchased from Aldrich Chemical Inc., Lancaster Synthesis Inc. and TCI America, respectively. Several luminescent materials were used, including a conjugated polymer poly(3-*n*-butyl-*p*-pyridyl vinylene) (Bu-PPyV) and organic dyes: coumarin 6 (C6), coumarin 47 (C47) and nile red. The green dye C6 and the blue dye C47 were purchased from Lambda Physik Inc. Nile red was purchased from Aldrich. Bu-PPyV was synthesized by cross-coupling the corresponding 2,5-dibromopyridine and E-1,2-bistributylstannylethylene in the presence of a palladium catalyst. M_W was determined to be 5000-7000 g/mole by gel

Hole-Transport Polymer: PVK

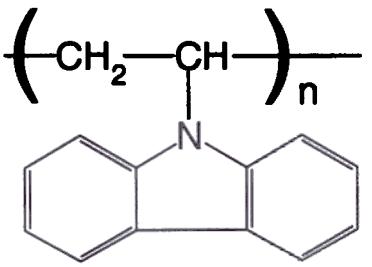

Electron-Transport Molecules:

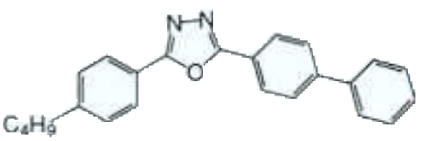

PBD

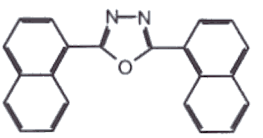

BND

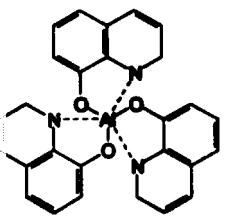

Alq

Emitters:

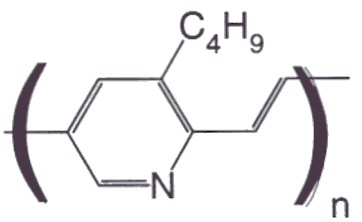

Bu-PPyV

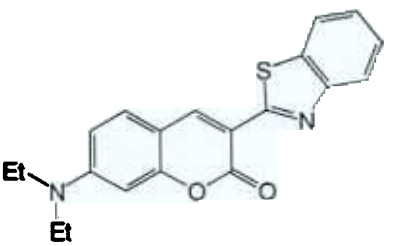

C6

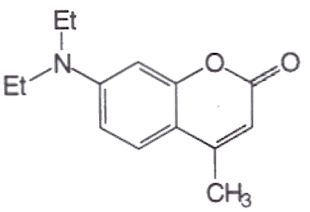

C47

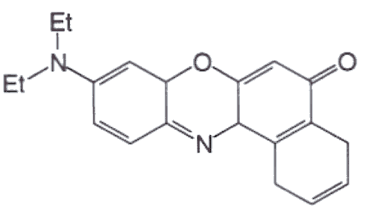

Nile Red

Fig. 3.1: Chemical structures of various compounds used in this thesis work.

permeation chromatography (M_w/M_n=1.9). More details of synthesis and its photophysical properties can be found in Ref.[1-4]. The synthesis and the M_w measurement were carried out by Dr. J. Tian in Prof. M. Thompson's and Prof. R. Register's labs at Princeton.

Preparation of Blend Solutions

In this thesis, the composition PVK:PBD:coumarin 6 (C6) (100:40:0.3 by weight) is used frequently. In the following, it is used as an example to explain how the solutions are prepared. Solutions of other compositions are similarly prepared. All the following steps were carried out in a chemical fume hood in air.

1. Determine the desired composition of the solution, for example, PVK:PBD:C6 of 100 mg:40 mg: 0.3 mg in 7.5 ml chloroform.
2. Use a balance (precise to 0.1 mg) to weigh chemicals.
3. Since the amount of C6 in the solution is small, the solution of C6 is prepared separately for a better accuracy. Therefore two solutions are made separately:
   solution 1: weigh 100 mg PVK and 40 mg PBD into a glass vial (rinsed by chloroform first). Measure 6.5 ml chloroform using a graduated cylinder and add it into the vial.

   solution 2: weigh 6 mg of C6 into another glass vial. Add 20 ml of chloroform. The concentration of this solution is then 0.3mg/ml.
4. Shake C6 solution and wait till it is fully dissolved in chloroform as observed by eye through the glass. Then use a micropipet (precise to tens of μl) to get 1 ml of solution 2 and add it into solution 1. The final solution therefore contains 100 mg of PVK, 40 mg of PBD and 0.3 mg of C6 in 7.5 ml chloroform.

7 Use a magnetic stirbar to stir the final solution at room temperature for ~20 minutes until the polymer PVK is fully dissolved and a clear (but highly fluorescent in green) solution is obtained.

8. Get another small glass bottle and rinse it twice with chloroform and blow dry. a syringe and a 0.45μ filter to filter the stirred solution into the new cleaned glass vial.

9 Store the solution thus made in the nitrogen dry-box for use. It is found from the device quality and film characteristics that the quality of the solution thus made and stored is nearly the same for at least two weeks. 7.5 ml is roughly enough for spin-coating 10 pieces of 1.25" × 1" ITO/glass substrates.

All the materials were used as received without further purification. The purity of dyes and oxadiazoles specified by the vendors are >99%. In our standard testing device, ITO/PVK:PBD:C6 (100:40:0.3 by wt., ~1050 Å)/Mg:Ag/Ag made on oxygen plasma-treated ITO (Section 3.3), the external quantum efficiency varied from 0.8% to (most often ~1%) from run to run. The same variation occurred in devices made from different batches of materials purchased, indicating that the quality of materials from the vendors is reliable.

Spin-coating and Measurement of Film Thickness

The film thicknesses are measured by either a Dektak stylus profilometer or an ellipsometer. To use the stylus profilometer, a polymer film is first scratched by hand with the dull side of a razor blade to produce a trench and is then scanned by the stylus tip to detect the depth of the trench, i.e. the film thickness. Because there is a problem with the stylus scratching into the soft organic films, it is difficult to measure a thin film of ≤1000 Å with an accuracy within 100 Å. The ellipsometer measures the thickness of such thin films more accurately and gives more repeatable results, but it usually requires a reflective

substrate. Because the thickness profiles scanned by Dektak for films spin-coated onto glass, ITO/glass or Si substrates from our blend solutions under the same condition are nearly the same, the combination of silicon substrates and ellipsometry has been routinely used to calibrate the film thickness vs. the concentration and the spin rate every time a new batch of solutions are made

To get a uniform film over the whole surface, it is necessary to drop the polymer solution to cover the whole substrate surface before spin-coating. Otherwise the increased viscosity of the polymer solution with the evaporation of the low-boiling-point solvent carrier during spin-coating will limit the uniform area of films to an area only slightly larger than the area covered by the solution prior to spin-coating. The variation of film thickness measured by ellipsometry at different spots near the center of the Si substrate (analogous to the center area of the ITO/glass substrate where devices are made) is within 50 Å for a ~1000 Å thick film coated from dilute solutions (<20 mg/ml). The variation becomes larger when the solution concentration and the film thickness increase (e.g. ~100 Å for a ~2000 Å thick films and ~250 Å for a ~4000 Å thick film). Due to the geometrical effect of spin-coating on a rectangular substrate, the uniformity of film thickness near the edges of the substrate is limited.

The solution composition in the previous section (i.e. PVK:PBD:C6 100:40:0.3 by wt.) will give a uniform film of ~1050 Å at the spin rate of 4000 rpm. The thickness of the spin-coated film mainly depends on the solution concentration and the spin rate. Fig. 3.2(a) shows the dependence of film thickness on the PVK concentration and the spin rate. Adding PBD or other molecules will slightly change the conditions for a particular film thickness. For instance, at a fixed spin rate, the total concentration required to spin-coat a fixed thickness increases with the addition of molecules into PVK, as shown in Fig. 3.2(b). The information in Fig. 3.2 is a good starting point for finding out the concentration and speed conditions for a desired film thickness from a particular blend composition. It is usually easier to get uniform films using a spin rate above 2500 rpm.

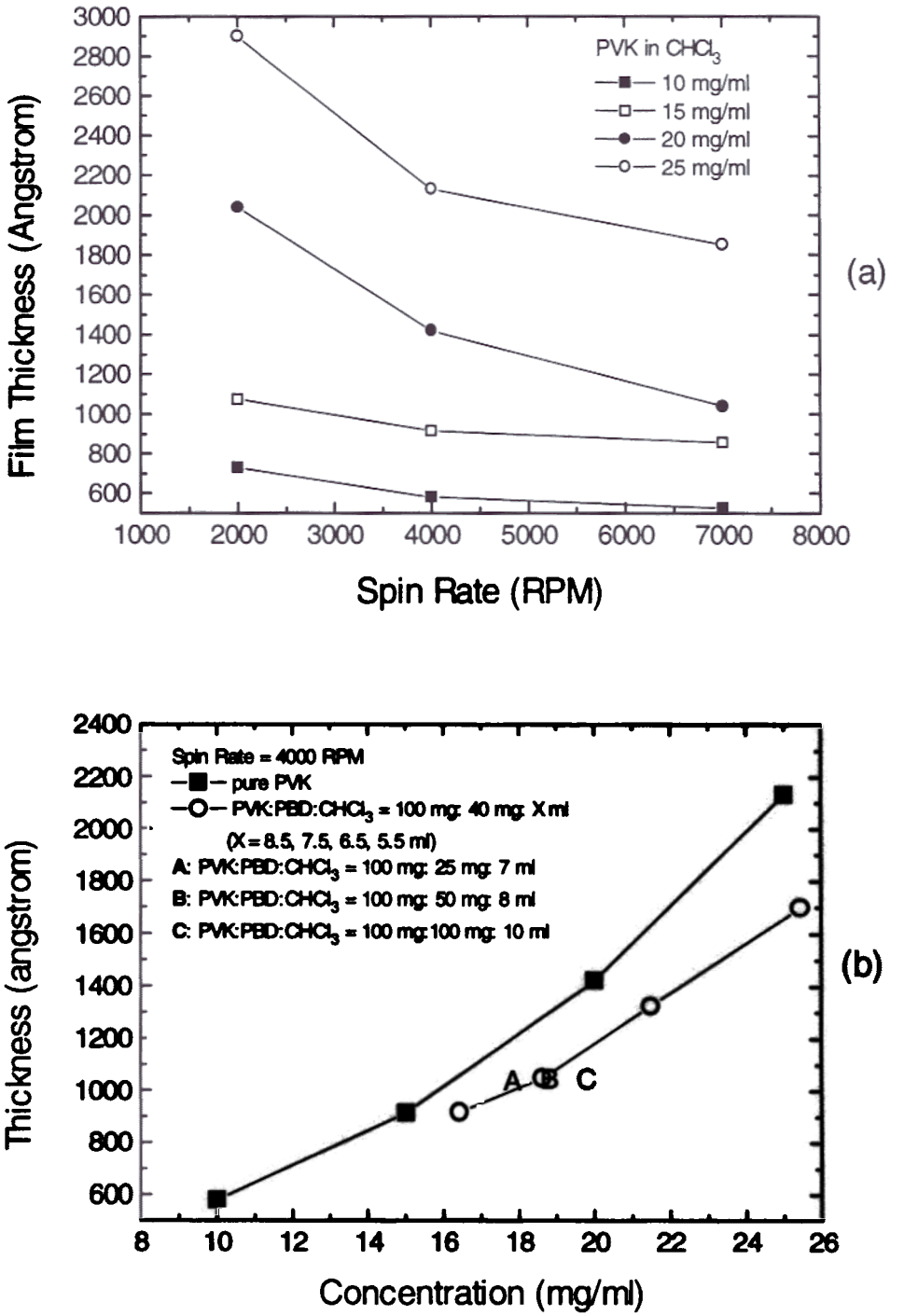

Fig. 3.2: (a) Dependence of the PVK film thickness on the solution concentration and the spin rate. (b) Dependence of the PVK:PBD blend film thickness on the solution concentration and the composition

Optical Characterization of Thin Films

To measure the optical properties, such as the absorption spectra and fluorescence (photoluminescence) spectra of polymer thin films, quartz substrates are used because the microscope glass slides and ITO-coated glass substrates absorb UV light substantially. The quartz substrates allows the spectral measurements to extend down to ~200 nm. The UV-VIS absorption spectra are measured on an AVIV 14DS spectrophotometer. The fluorescence spectra are measured on an Perkin-Elmer LS50 luminescence spectrometer. Both are shared equipment of the Chemistry Department, located in the basement of Frick Hall.

The transmittance spectra of ITO/glass or semitransparent metal thin films are measured by a Hitachi U-3410 spectrophotometer in the dual-beam mode. It is located in Prof. S. Wagner's lab.

Preparation of Blend Thin Films for TEM

As discussed in chapter 2, there are concerns of how different components in the blend distribute in the film, particularly in the case where there is more than one polymer component, such as PVK:Bu-PPyV blends. 1000 Å spin-coated polymer films are thin enough to be used in TEM if the substrate is removed. Since both polymers are composed of the same light atoms, i.e. C, H and N, there is no contrast between them under TEM. Therefore, it is necessary to "stain" one component to enhance the contrast. The much heavier iodine element is used to "stain" the Bu-PPyV in the blend. In the vapor of iodine, iodine can react with the pyridine group of Bu-PPyV and therefore attach to it [5]. Where there is Bu-PPyV in the blend, there would be iodine in a stained sample, which now gives enough contrast to be distinguished from PVK in TEM.

In addition to the contrast requirement, one also needs a free-standing polymer film rather than a film on a thick substrate, so that electrons can pass through. To get a free-standing polymer film, a "floating" technique is used [5]. In this technique, the

polymer film is spin-coated onto a substrate covered with a thin layer (~100 Å) of evaporated carbon film. On the substrate, the polymer film is scribed into small grids and the whole sample is then put into water to "float" off the small pieces of the polymer film. A metal grid is then used to "catch" one piece of the free-standing polymer film for TEM observation. This metal grid is pre-coated with a carbon network with holes of various sizes to facilitate the focusing of the TEM onto the polymer film.

3.2 Dry-Box Device Fabrication and Characterization System

Because of the use of reactive low work function metals for efficient OLEDs and reports of the degradation of luminescent organic materials used for OLEDs caused by either humidity or oxygen [6-9], the OLED device processing is carried out in a dry atmosphere. Fig. 3.3 shows the schematic diagram of our dry glove box system for device fabrication and characterization. This system consists of two glove boxes and two airlocks. Box 1 contains a spin-coater and a hot-plate/stirrer and is used for solvent-based chemical processing and spin-coating etc. Therefore a stainless steel box with a glass view window is used for its solvent resistance. Box 2 contains an evaporation chamber, an electrical characterization station and electrical feedthroughs for testing finished OLEDs. It does not involve chemical processing and therefore a cheaper transparent plexiglass glove box is used. The three-way Airlock 2 between Box 1 and Box 2 is used to transfer samples or small tools between boxes and in/out of both boxes. Airlock 1 is used for transferring larger tools in/out of Box 1. The back wall of Box 2 and the view window of Box 1 are removable so that the transfer of really large equipment or the cleaning of the interiors of the boxes and the evaporator chamber can be carried out. Both glove boxes of course are rarely opened. Each box or airlock is kept dry by flowing house nitrogen through and a positive pressure is maintained inside by mounting a check valve at the outlet of each box or airlock.

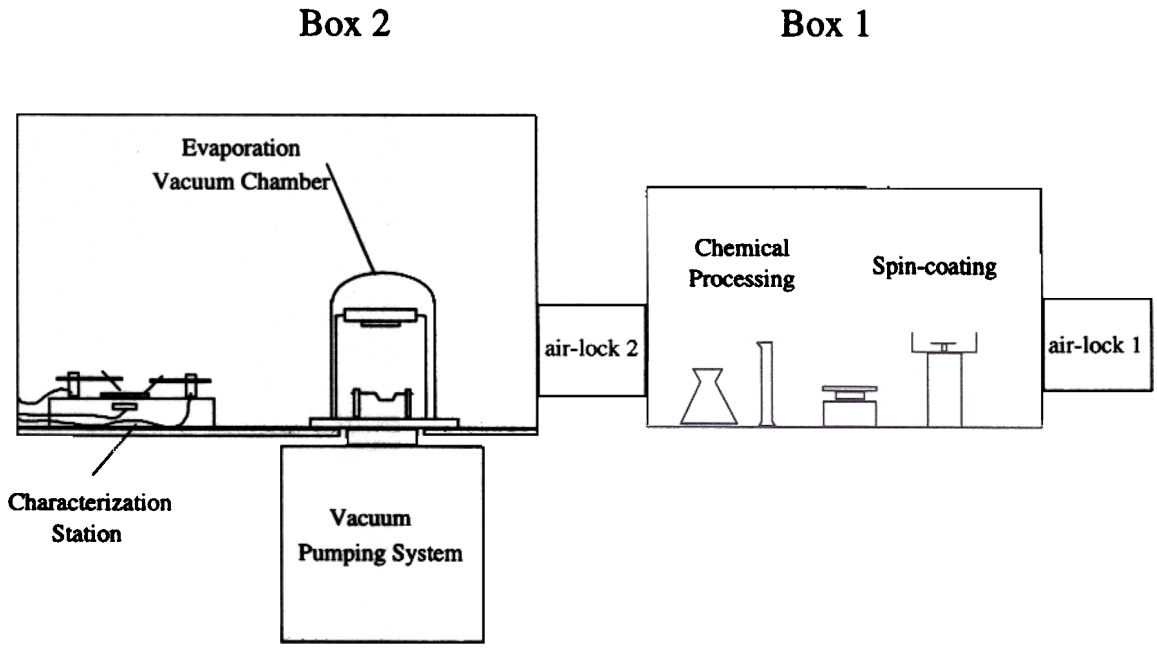

Fig. 3.3: Schematic diagram of the dry glove-box system for OLED fabrication and characterization.

The evaporator system is a home-made. The evaporation chamber is sealed inside Box 2 through an O-ring seal at the bottom of the baseplate. The chamber is also vented by nitrogen to avoid introducing air into the glove box and the chamber. The pumping system is composed of a diffusion pump backed by a 3-phase rotary vane pump and a liquid nitrogen cold trap. Usually, the chamber pressure rapidly drops to close to 10^{-6} Torr in a few minutes after the high vacuum valve between the diffusion pump and the chamber is open. Inside the chamber, two parallel pairs of electrodes are installed to allow the coevaporation of two metals simultaneously. A barrier plate is set between the two sources to prevent the cross-contamination. The sample holder is held ~25 cm above the source, mounted on a stand with a heater plate and thermocouples. A temperature controller is used to control the temperature of this heater plate. A cooling water pipe running through the plate allows fast cooling of this plate and the sample holder if they are heated. A shutter is placed close to the sample holder instead of to the sources, so that the evaporation rate can be preset before evaporation onto the sample. A crystal head with cooling water pipes is placed close to the sample holder but not blocked by the shutter, and is used to monitor the evaporation rates and film thicknesses. Two power supplies, again home-made from thermostats and 2-3 KVA low-voltage high-current transformers, are used to independently control the rate of each source through high-current feedthroughs.

3.3 Device Fabrication

Device Structures

The three kinds of device structures used are shown in Fig. 3.4. In all of these structures, ITO is the bottom hole-injecting anode and the top metal layer is the electron-injecting cathode. Because of the rather high inherent resistance of the organic thin films,

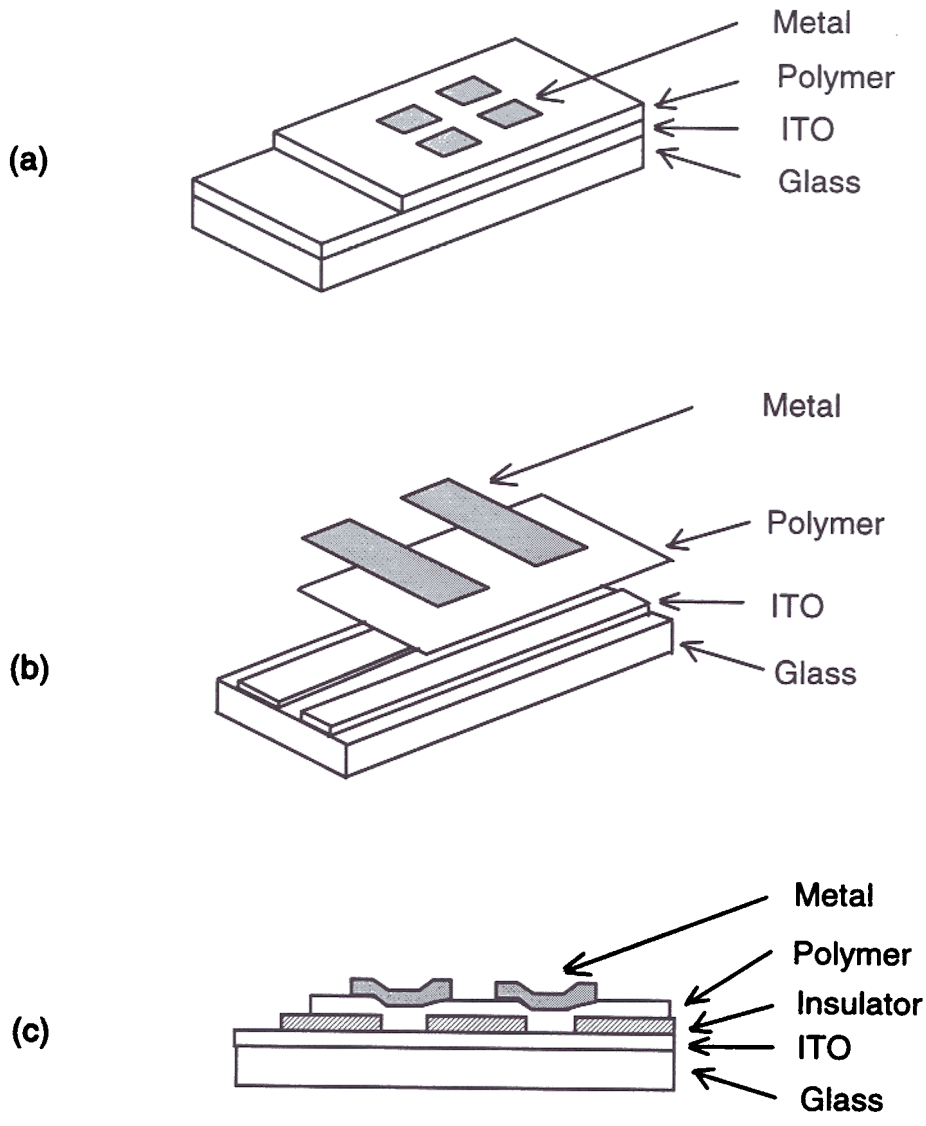

Fig. 3.4: Three different OLED device structures. (a) Structure A: with metal cathode patterned only. (b) Structure B: with both ITO anode and metal cathode patterned in stripes (c) Structure C: with a patterned insulating layer on top of ITO.

there is no need to pattern the organic layers to isolate each individual device The active device area is determined by the overlapping area of the anode and cathode contacts

Structure A, which involves the fewest processing steps, is used most often for device and material tests. Most of the device data presented in this thesis are from this structure, unless otherwise noted. The ITO layer and the organic layer are not patterned. The top metal cathode is the only patterned layer. The pattern is formed by a shadow

To probe each device, one probe is put on the common ITO anode and the other probe on the metal cathode. Because both the metal layer and the organic layer are soft, a soft gold wire bonded to a normal probe is usually used as the cathode probe. The fabrication of this structure involves the following steps:

(i) Prepare ITO/glass substrates.

(ii) Spin-coat the polymer thin films over the whole substrate surface and expose part of the ITO for contact by wiping off part of the organic layer with a Q-tip and the solvent.

(iii) On the sample holder, mount the shadow mask on top of the organic layer. The shadow mask usually contains a 3×3 array of 2 mm × 2 mm open holes Then load the sample holder into the evaporator.

(iv) Pump down the chamber to 10^{-6} Torr or even lower. Typically at least ~90 minutes were allowed between the loading of samples and metallization

(vi) Metallization.

In Structure B, the ITO layer is patterned into stripes and the top cathode stripes are deposited perpendicular to the ITO stripes through a shadow mask. The intersection of ITO stripes and metal stripes determines the active device area. In this structure, since the devices can be contacted outside the active device area, normal probes or wire-bonding can be applied to both anodes and cathodes When the devices are to be sealed with a cover glass plate and epoxy or adhesive, this structure is used so that the devices

can be contacted outside the sealed area. The general processing procedures for such a structure are as follows:

(i) Clean ITO/glass.

(ii) Photolithography and etching of ITO.

(iii) Remove photoresist and prepare ITO for devices.

(iv) Same device fabrication steps as for Structure A.

In Structure C, an insulator layer is deposited on top of the ITO layer and the device area is determined by the windows patterned in the insulating layer. Either the ITO or the metal layer is patterned to isolate each device. If the ITO is also patterned, the metal layer can be a continuous layer, saving the use of a shadow mask containing complicated patterns since the device pattern is now determined by the insulator layer and ITO, which can be patterned by lithography before the OLEDs are fabricated. example use of this structure is in Chapter 6, where it is used to integrate different polymer OLEDs on a single substrate. Processing steps are also described there.

Cleaning and Preparation of ITO

The ITO coated glass substrates used throughout this thesis are purchased from Donnelly Applied Films Co. in Colorado. It is of the grade used for passive matrix STN-LCD. The 1.1-mm-thick polished soda lime float glass is coated with a 200 Å SiO_2 barrier layer and a 1400 Å ITO film. ITO was sputtered from an In_2O_3-SnO_2 (90-10 wt.%) oxide target in an Ar/O_2 ambient at an elevated temperature (proprietary) using a planar DC magnetron sputtering system. The ITO was annealed in-situ during the deposition and no post-deposition annealing was performed. The measured sheet resistance and peak transmittance at ~550nm of the as-received ITO was 11Ω/square and ~90%, consistent with the vendor's specification of 10-15 Ω/square and >85%. polymer OLEDs are sensitive to the preparation of the ITO anode before the coating of

polymer layers [10,11]. The effects of various ITO treatments on the behaviors of polymer OLEDs will be discussed in Chapter 5. ITO preparation procedures we found most satisfactory so far are listed below:

1. Swab the ITO/glass with detergent:DI water (~1:10 in volume). The detergent used was Micro 8790 (International Products Co.) earlier and is changed to Tergitol (J.T. Baker) now. No notable difference was observed in devices between these two detergents.
2. Rinse in DI water.
3. Ultrasonic cleaning in detergent:DI water (~1:10 in volume).
4. Rinse in DI water and blow dry.
5. Degrease by flushing the ITO surface with convection flow in warm 1,1,1-trichloroethane.
6. Rinse in warm acetone.
7. Rinse in warm methanol.
8. Blow dry.
9. Subject the ITO/glass to an oxygen plasma treatment, at 25W (or ~50 mW/cm^2), 150 mTorr (base pressure ~5 mTorr), 25 sccm for ~4 minutes in a parallel-plate type plasma reactor configured in the reactive ion etching (RIE) mode. This is the optimal ITO treatment condition currently used. In some earlier generations of devices such as those presented in Chapter 4 and some in Chapter 5, the oxygen plasma treatment was carried out in a barrel-type plasma reactor (Plasmod produced by March Inc). On this machine, the power, flow rate and pressure are not well controlled. The estimated treatment conditions on the Plasmod reactor are ~300 mTorr (base pressure ~180 mTorr), flow rate ~50-60 sccm, <100 W for 5 minutes. The higher power used on the Plasmod leads to a bit higher drive voltage (2-3 V) on

the devices, but does not affect the quantum efficiency, as will become clear in Chapter 5.

Patterning of ITO by Wet Etching

The wet etching and processing for ITO are described below. Further references for more advanced ITO wet etching, such as the control of taper angles, could be found in Ref.[12]:

1 Clean ITO/glass as described previously without plasma treatment.
2. Spin-coat photoresist AZ1518 at 4000 rpm.
3. Bake in the oven at ~90°C for ~20 min.
4. Exposure ~10 sec.
5. Develop in AZ351 developer (AZ351:DI water 1:5).
6. Rinse in DI water and blow dry.
7. Etch ITO in a mixture $HCl:HNO_3:H_2O$ of 20:5:75 by weight at ~55°C. Adding a few drops of detergent into the etchant will help the wetting of the ITO surface and accelerate etching. The etching of 1400 Å ITO is usually completed in ~2 minutes.
8. Rinse in DI water and blow dry.
9. Use a multimeter to check the resistance of the etched areas to make sure the ITO etching is complete.
10. Remove PR with acetone

Deposition of Metal Alloys by Coevaporation

Many efficient OLEDs involve the use of reactive metals such as Mg, Li or Ca in the cathodes. To enhance the adhesion of such reactive metals to the organic films or to retard the corrosion by atmosphere, they usually are alloyed with another stable metal [13]. The metal alloy films are deposited by coevaporation from separate sources

controlled by independent power supplies. The alloy ratio is controlled by the evaporation rate of each metal and therefore the current from each power supply. Throughout the thesis, the Mg:Ag alloy is used most often, therefore it is used as an example to illustrate the coevaporation of an alloy. In our evaporator, the shutter is placed close to the sample holder so that the evaporation rate can be preset before the shutter is open. Only one thickness monitor is installed, therefore the control of the ratio between two metal evaporation rates is a bit tricky. The procedures are now listed below:

1. Place silver (Ag) in a tungsten (W) boat and Mg in a tantalum (Ta) boat. The Ta boat has a cover with holes smaller the Mg grains. The cover is to prevent the Mg grains popping out of the boat during the evaporation (actually sublimation). This occurs because the surface of Mg grains is usually more or less covered by magnesium oxide and the thermal expansion coefficients of Mg and magnesium oxide are different. When they are heated up, Mg erupts out of the oxide surface and the grains pop around like popcorn.
2. Pump down the chamber to $\leq 10^{-6}$ Torr.
3. Set the parameters of the thickness monitor to those of Mg.
4. Turn on the power supply to the Ag boat and adjust the current level to where Ag just melts and the thickness monitor shows a rate between 1-1.5 Å/sec under Mg parameters. Once the rate is stable in that range, keep the setup untouched.
5. Turn on the power supply to the Mg boat. When Mg is just heated up, the chamber pressure usually suddenly rises up to the 10^{-5} Torr range due to outgasing without any rate indicated on the thickness monitor. The pressure will come back down to the 10^{-6} Torr range and the evaporation rate on the monitor starts to rise. Adjust the current level to where the total rate on the thickness monitor shows a rate between 9-10 Å/sec.

6. Zero the thickness monitor and open the shutter to start the coevaporation of ~1200 Å Mg:Ag.
7. Turn off the power supply to the Mg boat. Reset the parameters of the thickness monitor to those of Ag.
8. Raise the current level to the Ag boat to get an evaporation rate of ~8-10 Å/sec for the evaporation of the ~ 800-1000 Å Ag cap (or passivation) layer.

Other alloy compositions, such as Mg:In (10:1), Al:Li (very low Li content), could also be deposited using similar procedures.

3.4 Device Characterization

The current-voltage (I-V) characteristics of the devices are measured using a Hewlett-Packard 4145B analyzer. The probing method for various device structures has been described in a previous section. Occasionally, the devices are found shorted initially with a steep linear I-V curve, particularly in larger devices. Most of the time, the shorted devices can be revived by gradually increasing the current compliance in the I-V scan. If the devices are just shorted by some local shorting paths, at some current levels, the shorting paths are burnt out and the devices again function normally. Of course, if the devices are seriously shorted by large-area defects, this burn-in trick will not work.

The light intensity is detected by a large-area (1 cm diameter) Si photodetector (PIN-10DP from UDT Sensors Inc.) operated under the photovoltaic (zero bias) mode, whose induced photocurrent is measured by a Hewlett-Packard 4140B picoampere meter. The photodetector is placed close to the bottom of the glass substrate (~3mm), collecting only the light emitted out of the backside of the glass substrate (1.1 mm thick). The total optical output power Q (measured in watts) is estimated by:

$$Q\,(W) = [I_{ph} / R(\lambda)] / G \tag{3.1}$$

I_{ph}(A): the induced photocurrent of the Si photodetector

$R(\lambda)$: the responsivity of the photodetector at the wavelenth range of the OLED, measured in A/W.

G: light collection efficiency

The collection efficiency is smaller than one because the collection solid angle is smaller than 2π due to the finite size of the detector, and because not all light is incident normal to the detector surface. Fig. 3.5(a) illustrates the measurement setup, with a distance d between the center of emitter surface and the center of the detector surface. θ is half the angle expanded by two lines connecting the center of the emitting surface to the edges of the detector surface. The angular dependence of the emission from a conventional OLED as shown in Fig. 3.4(a) has been previously experimentally measured to be very close to Lambertian emission [13-15]. That is, the angular dependence of the light intensity follows the $\cos\phi$ dependence, where ϕ is the angle between the normal of the emitter surface and the viewing direction. Assuming all light within the solid angle expanded by θ is collected by the detector, the signal in the detector will show a $\sin^2\theta$ dependence when the total light output is fixed and the distance d is varied. In Fig. 3.5(b), the measured signal is compared with the $\sin^2\theta$ function. Clearly, at smaller distance ($d \leq 10$ mm), the measured signals apparently deviate from the $\sin^2\theta$ dependence. The large deviation at smaller distance and therefore larger θ indicates the effects of the incident direction of light on the collection efficiency. At larger distance ($d \geq 20$ mm), the measured signals match the $\sin^2\theta$ dependence fairly well, since all light is now within a small solid angle and is rather normal to the detector surface. From the signal detected at a larger distance and the $\sin^2\theta$ dependence, the total light output is calculated. By comparing the calculated total light output with the measured signal, the collection efficiency of our setup is estimated to be ~70%. The external quantum efficiency η_e, photons emitted in the forward direction per injected electron, is estimated from the following equation:

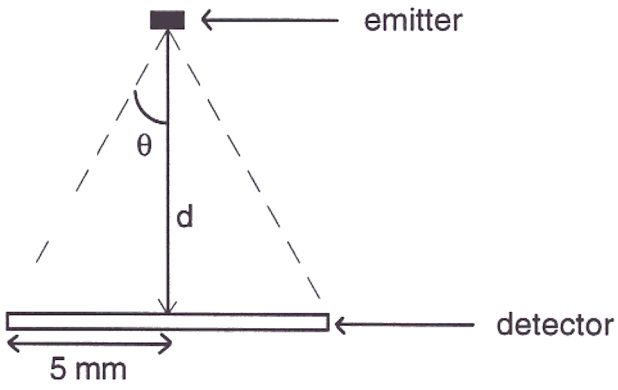

(a)

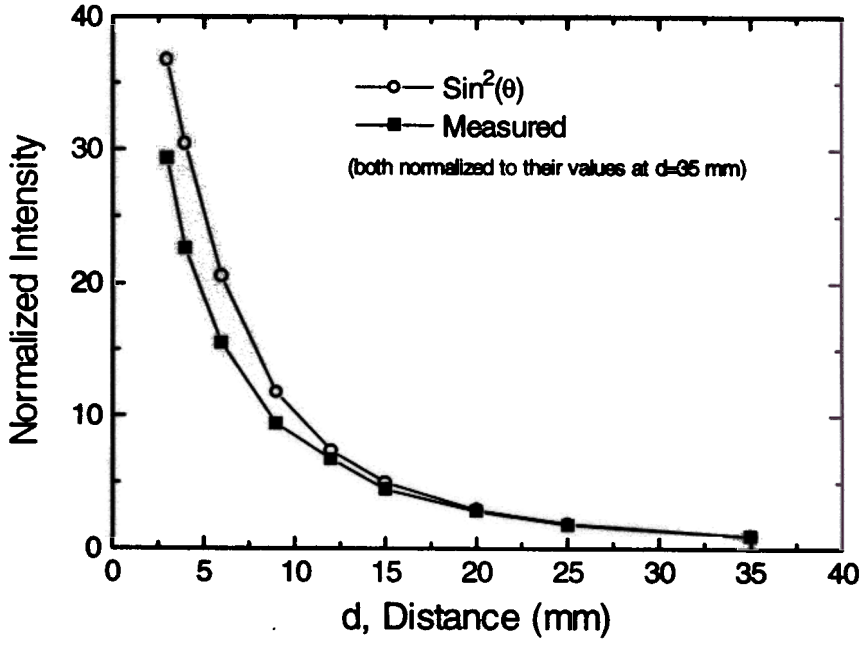

(b)

Fig. 3.5: (a) The relative position between the OLED and the detector. (b) Measured light output and $\sin^2\theta$ vs. d.

η_e (photon/electron) $[Q / h\upsilon] / [I_{OLED} / e]$

$h\upsilon$ (eV): photon energy

I_{OLED} (A): OLED drive current

The electroluminescence spectra of the OLEDs are recorded by an EG&G monochromator connected to an thermoelectrically cooled Electrim CCD camera. wavelengths are calibrated by spectral lines of mercury and a He-Ne laser. The spectral response of the system is calibrated by a quartz-tungsten-halogen lamp with its known spectrum.

3.5 Photometry vs. Radiometry

Radiometry is the science of the measurement of electromagnetic (EM) radiation. It is purely physical and covers the entire EM spectrum. In an electronic display, however, how the human eyes record optical radiation is more relevant than the absolute physical values. Photometry is the quantitative measurement of radiant flux in relation to its ability to stimulate physiological and psychological sensations of "brightness" in human eyes. It is limited to only a small portion of the EM spectrum, i.e. visible light from 380 nm to 780 nm [16,17]. To this end, the response of the "standard" light adapted eyes (photopic vision) has been defined. Fig. 3.6 shows such a standard normalized photopic curve $V(\lambda)$, which was obtained by making comparative recognition measurements on a number of observers and indicates the effectiveness of each wavelength in evoking the brightness sensation. A human eye is most sensitive to green light and its sensitivity drops by many orders of magnitude at the extreme of red and blue. Having this photopic curve, the photometric quantities are obtained from radiometric ones by superimposing the photopic function on corresponding radiometric quantities. The general conversion formula is

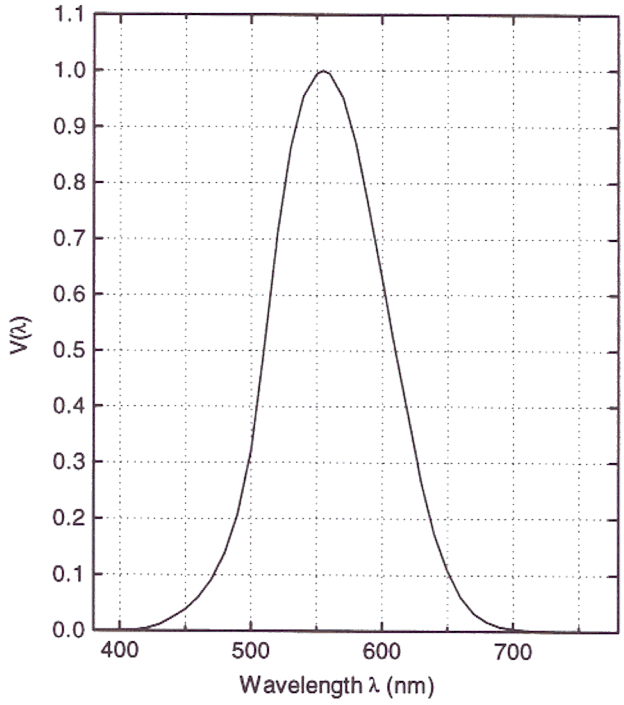

Fig. 3.6: Normalized CIE photopic curve V(λ) for "standard" light adapted eyes.

$$\text{Photometric quantity} = C \int (\text{spectral radiometric quantity})\, V(\lambda)\, d\lambda$$
$$= \int (\text{spectral radiometric quantity})\, K(\lambda)\, d\lambda \qquad (3.3)$$

$C = 683$ lumen/watt

$K(\lambda) = C \times V(\lambda) = 683\, V(\lambda)$ (lumen/watt)

$K(\lambda)$ is the *luminous efficiency* of the human visual system. *Luminous efficiency* is the ratio of the photometric output to the radiometric input and is defined for monochromatic light. The *lumen* or *lm* is the unit of luminous flux, corresponding to radiant flux (watt) in radiometry. At the peak wavelength of the photopic curve, i.e. yellow-green light 555 nm, 1 light watt is equivalent to 683 lumens, While for 630 nm red light and 470 nm blue light, 1 light watt only corresponds to 180 lumens and 62 lumens, respectively.

Luminous intensity, identical in concept to radiant intensity, is the total number of lumens per unit solid angle from a source emitted in a given direction. The unit of luminous intensity is therefore *lm/steradian*, or more often called *candela* (*cd*). It is most often used to deal with point sources such as inorganic LEDs. Inorganic LEDs are usually specified by their luminous intensity, most often in *millicandelas*. The efficiency of an inorganic LED is often specified by *cd/A* (candela per ampere).

The photometric quantity most used in the specifications of an electronic display is, however, the *luminance*, which is the luminous intensity of a light emitting or reflecting surface in a given direction, per unit projected area of that surface viewed from that direction. The luminance directly corresponds to what the eye perceives as the brightness of a surface. Therefore, *brightness* is frequently used as synonymous with luminance. The unit of luminance is *lm/(steradian·m^2)* or simply *cd/m^2* (= nits). The luminance (or brightness) level of a diplay or a piece of white paper under room light is typically on the order of 100 cd/m^2. The brightness level of a clear sky in daylight (not looking directly at the sun!) and a fluorescent lamp are about 3000 and 5000-6000 cd/m^2, respectively. The

tolerance limit for human eyes is ~100,000 cd/m^2, and the visible threshold of eyes in darkness is 0.00001 cd/m^2.

For an ideal diffuse light-emitting or reflective surface with an area A, the angular distribution of luminous intensity obeys Lambert's law:

$$I(\theta) = I_0 \cos\theta$$

where θ is the angle between the normal of the emitting surface and the viewing direction, and I_0 is the luminous intensity along the normal to the (plane) surface. Since the projected area of the surface along the angle θ is (A $\cos\theta$), for such a surface, the luminance (brightness) is constant I_0/A, independent of the viewing angle. Therefore, there will be no viewing angle problem for such an emitting surface. The angular dependence of the emission from a conventional OLED as shown in Fig. 3.4(a) has been previously experimentally measured to be very close to such Lambertian emission [13-15]. The wide viewing angle has actually been considered as an important advantage of OLED displays.

Knowing the angular distribution of OLED emission, one can calculate the luminance L (cd/m^2) from the measured total power Q (W) and vice versa. For simplicity, assume a monochromatic OLED of area A, with emission wavelength λ, and measured total optical power Q, the relationship between Q and the luminous intensity along the normal I_0 is:

$$2\pi \int I_0 \cos\theta \sin\theta \, d\theta = \pi I_0 = 683 \, Q \, V(\lambda)$$

therefore,

$$L \, (cd/m^2) = I_0 / A = 683 \, Q \, V(\lambda)/(A \, \pi)$$

In general, this would be

$$L\ (cd/m^2) = I_0 / A = 683\ Q\ M/(A\ \pi) \tag{3.7}$$

$$M = \int S(\lambda)\ V(\lambda)\ d\lambda\ /\ [\int S(\lambda)\ d\lambda] \tag{3.8}$$

$S(\lambda)$ = radiometric spectrum of the light emitter

Another important parameter for an electrically powered light emitter or an electronic display is the power efficiency. In photometry, it is specified by the *luminous efficiency*, the total number of lumens generated from one watt of electric power, with the unit *lm/watt*. In an OLED, assuming a total optical power Q (W) measured at the current I (A) and voltage V (V), the luminous efficiency is calculated by:

$$\text{Luminous efficiency (lm/W)} = 683\ Q\ V(\lambda)/(I \cdot V) \tag{3.9}$$

(for monochromatic light)

$$= 683\ Q\ M\ /\ (I \cdot V)$$

(in general) (3.10)

The typical luminous efficiency of fluorescent lamps is 50-100 lm/watt, ~10 lm/watt for CRTs and ~1-3 lm/watt for AMLCDs.

References

[1] M.J. Marsella and T.M. Swager, Polymer Preprints. **33**(1), 1196 (1992).

[2] J. Tian, M.E. Thompson, C.C. Wu, J.C. Sturm, R.A. Register, M.J. Marsella and T.M. Swager, Polymer Preprints **35** (2), 761 (1994).

[3] J. Tian, C.C.Wu, M.E. Thompson, J.C. Sturm, R.A. Register, M.J. Marsella and T.M. Swager, Adv. Mater. **7**, 395 (1995).

[4] J. Tian, C.C. Wu, M.E. Thompson, J.C. Sturm and R.A. Register, Chem. Mater. **7**, 2190 (1995).

[5] Y. Liu, W. Zhao, X. Zheng, A. King, A. Singh, M.H. Rafailovich, J. Sokolov, K.H. Dai, E.J. Kramer, S.A. Schwarz, O. Gebizlioglu and S.K. Sinha, Macromolecules **27**, 4000 (1994)

[6] D.G.J. Sutherland, J.A. Carlisle, P. Elliker, G. Fox, T.W. Hagler, I. Jimenez, H.W. Lee, K. Pakbaz, L.J. Terminello, S.C. Williams, F.J. Himpsel, D.K. Shuh, W.M. Tong, J.J. Jia, T.A. Callcott and D.L. Ederer, Appl. Phys. Lett. **68**, 2046 (1996)

[7] F. Papadimitrakopoulos, X.M. Zhang, D.L. Thomsen and K.A. Higginson, Chem. Mater. **8**, 1363 (1996)

[8] L.J. Rothberg, M. Yan, F. Papadimitrakopoulos, M.E. Galvin, E.W. Kwock and T.M. Miller, Synthetic Metals **80**, 41 (1996)

[9] P.E. Burrows, V. Bulovic, S.R. Forrest, L.S. Sapochak, D.M. McCarty and M.E. Thompson, Appl. Phys. Lett. **65**, 2922 (1994)

[10] C.W. Tang, S.A. VanSlyke and C.H. Chen, J. Appl. Phys. **65**, 3610 (1989)

[11] C.C. Wu, C.I. Wu, J.C. Sturm and A. Kahn, *Appl. Phys. Lett.* **70**, 1348 (1997)

[12] J.H. Lan, J. Kanicki, A. Catalano, J. Keane, W.D. Boer and T. Gu, J. Electron. Mater. **25**, 1806 (1996)

[13] C.W. Tang and S.A. VanSlyke, Appl. Phys. Lett. **51**, 913 (1987)

[14] N.C. Greenham, R.H. Friend and D.D.C. Bradley, Adv. Mater. **6**, 491 (1994)

[15] D. Braun, E.G.J. Staring, R.C.J.E. Demandt, G.L.J. Rikken, Y.A.R.R. Kessener and A.H.J. Venhuizen, Synth. Metals **66**, 75 (1994)

[16] J.W.T. Walsh, Photometry, Third. ed., Constable & Co., London (1958)

[17] T.N. Cornsweet, Visual Perception, Academic Press, New York (1970)

Chapter 4

LEDs from Single-layer Doped Polymers

4.1 Introduction

In this chapter, electroluminescent devices made from single-layer doped polymer blend thin films are discussed. The active organic layer consists of the hole-transport polymer poly(N-vinylcarbazole) (PVK) containing dispersed electron-transport molecules, as well as different fluorescent small molecules or polymers as emitting centers to vary the emission color. Both the photoluminescence and electroluminescence properties are extensively studied. We present information relating to the optimization of this class of devices by systematically studying the relation between the device performance and the compositions of the blends. By correlating device characteristics and material properties, we also seek to understand the behavior of carriers inside these devices.

In this chapter, we will use the PVK:Bu-PPyV and PVK:PBD:Bu-PPyV blends as model systems for detailed discussions. The behavior of the luminescent polymer Bu-PPyV and other organic dye emitters used are very similar. The conclusions drawn from the model system can therefore be generalized to other material systems in this chapter when appropriate.

4.2 Characteristics of the PVK:Bu-PPyV and PVK:PBD:Bu-PPyV Blends

4.2.1 Optical Properties of Blend Thin Films

Fig. 4.1(a) shows the ultraviolet-visible (UV-VIS) absorption spectra of thin films of PVK, PBD, and Bu-PPyV. Both PVK and PBD have an absorption onset wavelength around 360 nm. The absorption onset of Bu-PPyV is at a longer wavelength of 520 nm. Clearly, PVK and PBD have higher optical energy gaps than Bu-PPyV. The absorption spectra of PVK:PBD:Bu-PPyV blend thin films of various compositions are displayed in Fig. 4.1(b). The absorption spectra of the mixtures keep all the features of each individual component and show a proportional contribution from each component. These and the lack of new features in the electronic absorption indicate that the basic structures of the individual components are preserved at the molecular level and that there are no ground-state interactions between components.

Since Bu-PPyV is added into the PVK or PVK:PBD host to act as the emitting centers, we were then interested in its emission behavior in the host. In the photoluminescence (fluorescence) experiments, two excitation wavelengths, 340 nm and 420 nm, were used to extract different information about the optical properties of the blend thin films. 420 nm is chosen because it is close to the absorption peak of Bu-PPyV and is below the absorption onset energy of PVK and PBD. By exciting the thin films at 420 nm, it is ensured that only Bu-PPyV chromophores are excited. 340 nm is used because its photon energy is beyond the PVK and PBD absorption onset energies and there is minimal absorption from Bu-PPyV chromophores in the blend with low or medium Bu-PPyV concentration. Therefore, most of the 340 nm optical energy is absorbed by PVK or PBD in such blends.

The PL spectra of PVK:Bu-PPyV thin films with different Bu-PPyV concentrations using an excitation wavelength of 420 nm are shown in Fig. 4.2(a). In blends with low Bu-PPyV contents, a strong green emission is observed. When the Bu-PPyV content increases above several percent, the PL spectrum gradually becomes

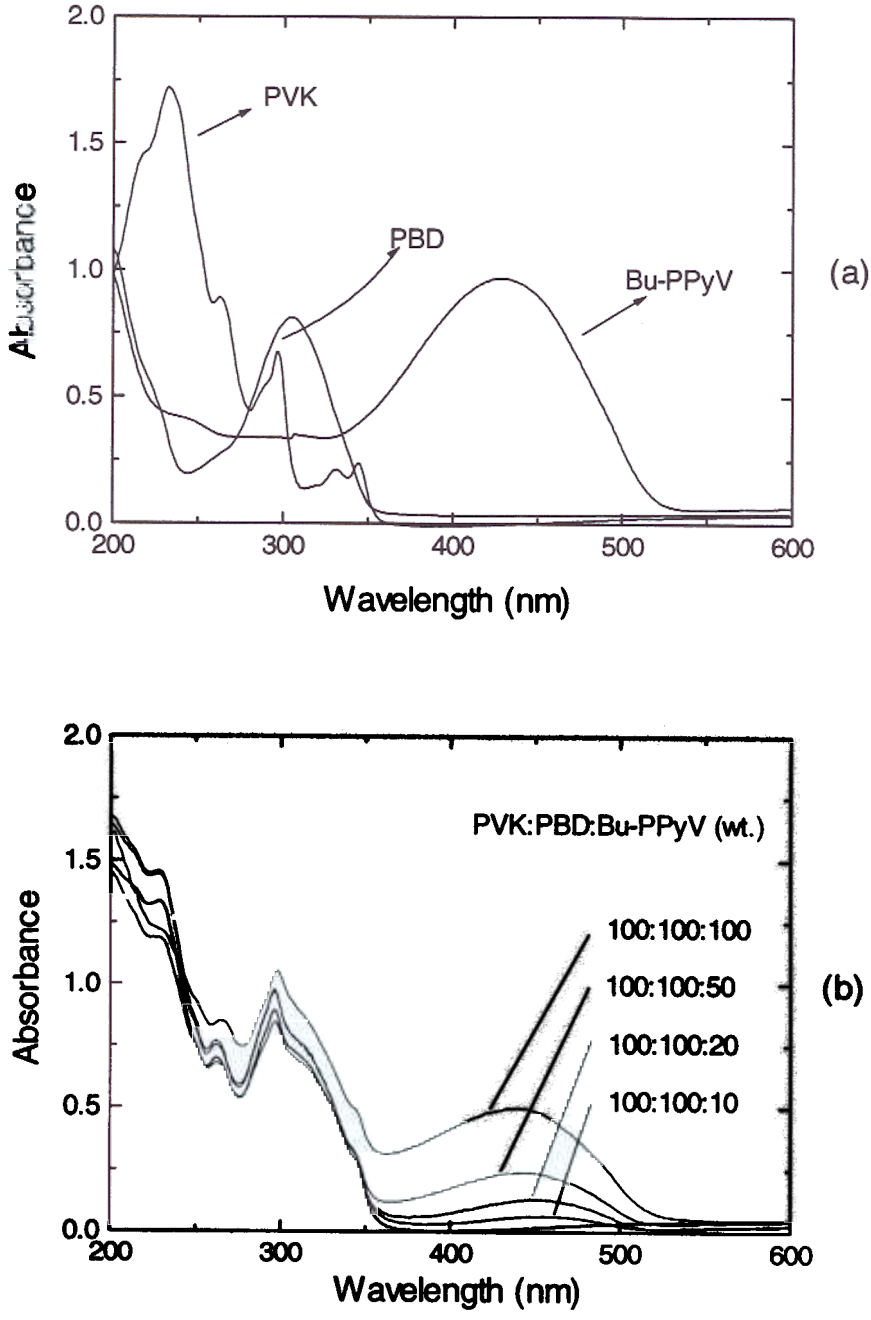

Fig. 4.1: UV-VIS absorption spectra of (a) PVK (900-1000Å), PBD, Bu-PPyV (900-1000Å), and (b) PVK:PBD:Bu-PPyV blend thin films (all 900-1200Å). The PBD spectrum was taken from its dispersion in inert poly(methyl methacrylate) (PMMA), PBD:PMMA (100:100 wt., 900-1000Å). PMMA shows no absorption at >200 nm.